6

Instrumentation for Intense Laser Field Effect Studies in a Liquid Microjet in Vacuum

6.1 Plasma from liquid droplets

In the previous chapters we studied the interaction of laser pulses with nanomaterials at moderate laser intensities and that with water at high laser intensities. As the intensity of the femtosecond laser pulse increases to 10^{16} W/cm^2 and beyond, the extremely intense laser-matter interaction will give many interesting effects. The production of x-rays, γ-rays, highly energetic ions and electrons is the result of such an excitation. Higher the input laser intensity, more and more new nonlinear effects will become apparent. One of the novel targets for intense laser-matter interaction is the liquid microdroplet. They are intermediate in size between gas and solid targets [Symes et al.] falling in the wavelength scale of the interacting laser. Due to the small size the droplet plasma gets heated up without losing energy to the cold bulk plasma, and hence under identical irradiation conditions droplets will attain relatively higher temperatures. The spherical geometry of the droplets facilitates internal focusing within the droplet, enhancing the internal intensity by two orders of magnitude or more. These targets are thus attractive in the using lower intensity laser pulses they will provide an opportunity to observe phenomena that are realizable only at higher laser intensities with normal targets. For instance, if the laser intensity available with us is of the order of 10^{15} W/cm^2 , the focused intensity will be 10^{17} W/cm^2 opening up experimental possibilities in the higher intensity regime. In this chapter we report the design and development of an experimental facility required for studying the interaction of liquid droplets with intense laser pulses in vacuum. At

present we produced a liquid microjet using a capillary system, but with some modifications it is possible to produce the droplets for future experiments.

6.2 Vacuum chamber with differential pumping

At high laser intensities air itself will act as a nonlinear medium, which can be prevented in a vacuum environment. For x-ray emission studies a minimum working pressure of 10^{-3} Torr is necessary to prevent air from affecting the plasma expansion or absorbing emissions from the plasma. Vacuum is essential for the plasma to attain high temperatures as well, since energy transfer to the ambient air has to be avoided. For detecting ions a vacuum of the order of 10^{-7} Torr will be necessary. Since we design the vacuum chamber to introduce liquid droplets, the chamber has to handle injected liquid load also. This situation is somewhat unconventional because the liquid will easily evaporate in vacuum increasing the pressure by a few orders of magnitude. For handling the injected liquid load, our chamber is initially evacuated to a pressure of $1x10^{-6}$ Torr by using a turbo molecular pump. A differential pumping set up is used to collect the liquid out of the chamber before it evaporates completely. The details of the chamber and the differential pumping are given in the next sections. With an ethanol jet introduced to the chamber we could attain a working pressure of $1x10^{-3}$ Torr which was sustainable for several hours. In the present set up no cryopumping is used.

6.2.1 Design of the vacuum chamber

. Even though the liquid volume injected to the chamber is only a few microliters per second, the number of molecules introduced is as high as 10^{19} molecules per second. In order to keep the working pressure in the chamber sufficiently low, the number of molecules per unit volume should be kept to a minimum. In principle one can use vacuum pumps of very high pumping capacity for this purpose. Using cryopump is one good option while handling a very high

vapour load. Another option is to use a big chamber so that the number of molecules per unit volume becomes less. In other words, the chamber will be acting as a buffer holding the liquid vapor before it is pumped out, while keeping the pressure sufficiently low. This method is useful where the use of a cryopump is not feasible. In our case a turbo molecular pump itself is found to handle the liquid load satisfactorily. The chamber is of 40" diameter and 15" height, and has a volume of approximately 300 litres. It is made of SS304.

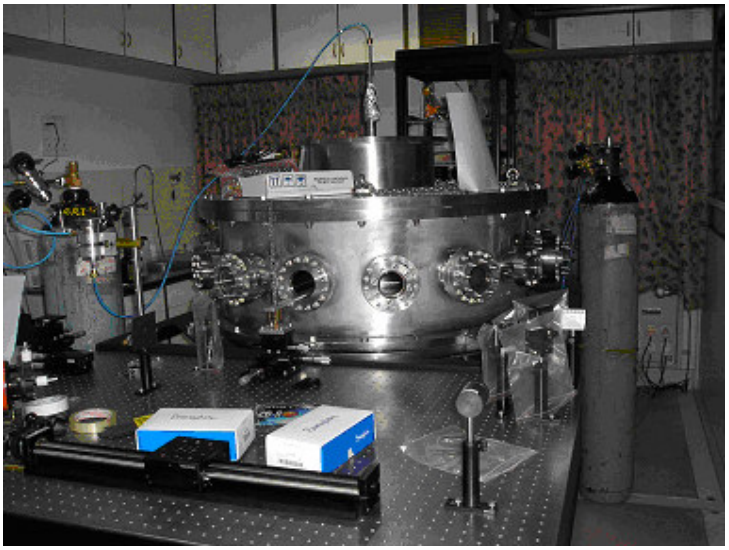

Figure 6.1: The vacuum chamber with the liquid inlet coupled from the top

There are 16 ports along the periphery of the chamber as shown in figure 6.1. All the ports are centered to the interaction region in the center of the chamber. The ports are fixed at an angular separation of 22.5^0 from each other so as to facilitate angle dependent detection. There are 11 view ports in the central port plane. The x-ray cut off of the view ports is given in figure 6.3. The view port material, BK7, cuts off X-rays with energies below 15keV. Two of the ports are for connecting the vacuum gauges. There is an electric feedthrough connection port. One port is included as an option for liquid nitrogen feedthrough in case cryo cooling is used in future to deposit the liquid vapor. Another port is included for

future expansion of the chamber with the time of flight module for detecting charged particles.

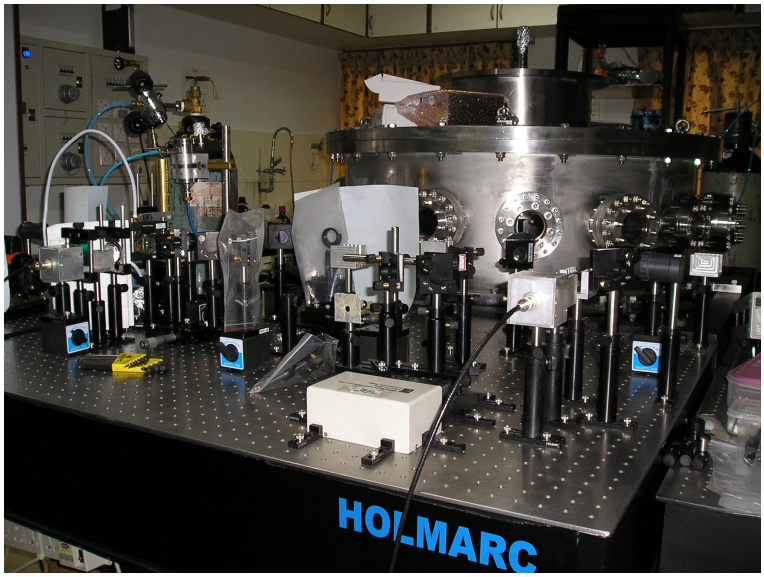

Figure 6.2: The chamber with optics aligned for recording the laser pulses. The set up for the water jet studies described in chapters 4 & 5 can be seen in the left foreground.

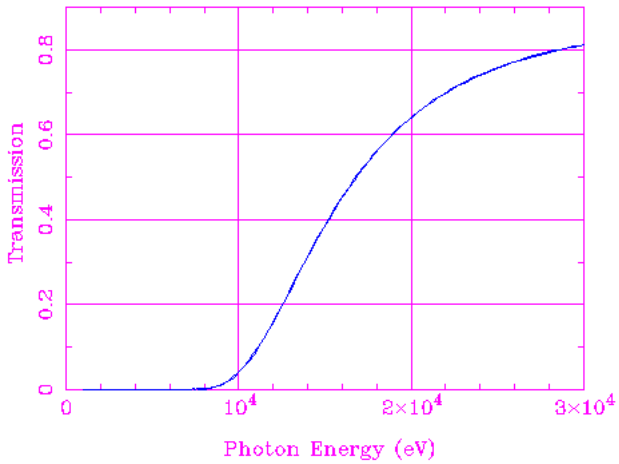

Figure 6.3: The typical transmission spectrum of BK7, the view port material, for x-rays.

The chamber is pumped using a turbo molecular pump backed by a dry pump. Thus the pumping system is oil free. The turbo molecular pump is connected to the chamber through an electro-pneumatically actuated gate valve, for isolating the pump from the chamber. The arrangement is seen in figure 6.4. The gate valve is actuated by connecting a nitrogen cylinder to provide compressed air at a maximum of 5 bar. Another electro-pneumatically actuated gate valve connects the dry pump to the turbo molecular pump. A parallel adapter is connected to the nitrogen cylinder so that the same pressure can be applied to both of the gate valves. The gate valves are set such that when power is given to the solenoid, the valves are in the open position. When power to the solenoid is cut off, the gate valves will be closed. Since gate valves having the same operating ranges of actuating air pressure can be driven in parallel, only one nitrogen cylinder is required to drive them. This method is useful when a compressed air supply line is not available.

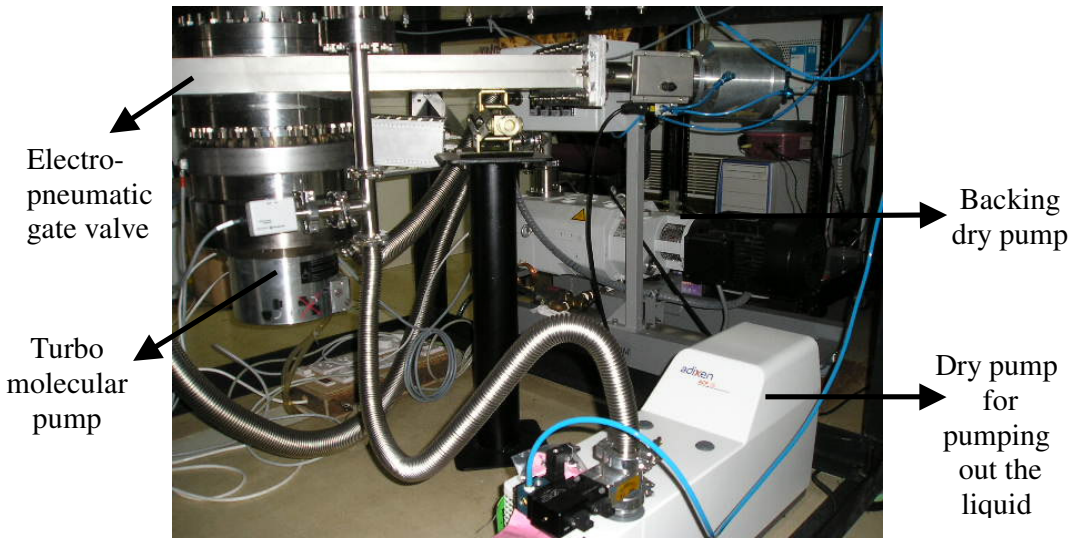

Figure 6.4: Bottom side of the chamber with the differential pumping arrangement. The turbo molecular pump and the gate valve also are seen.

There is a provision to connect the backing pump directly to the chamber so that while roughing the chamber (i.e. bringing the chamber to a pressure $<5x10^{-2}$ Torr) the port of the turbo molecular pump is not open to the chamber. The combination of a small electro-pneumatically actuated gate valve and a manually controlled gate valve allows switching between these two pumping lines. The turbo molecular pump has a pumping capacity of 1900 l/s, and the backing dry pump has a pumping capacity of 833 l/min. Both the turbo molecular pump and the dry pump are water-cooled.

The roughing pump alone will evacuate the chamber to $<5x10^{-2}$ Torr in 5 minutes. With the turbo the chamber pressure will be reduced to $<5x10^{-6}$ Torr in another 15 minutes. A Pirani gauge is used to measure the rough vacuum. The measuring range of the Pirani gauge is from 750 Torr to $3.75x10^{-4}$ Torr. A Pirani gauge essentially uses the thermal conduction of the gas to measure the pressure. The gauge head is placed around a heated wire that is exposed to the gas. The resistance of the wire is temperature dependent. When the gas molecules collide with the wire its temperature and hence the resistance decreases. When the pressure in the chamber decreases, the number of colliding molecules decreases and hence the temperature of the wire increases. A calibration of this temperature dependent resistance makes it useful for pressure measurement. Lower pressures are measured using a cold cathode gauge, which offers a measuring range of $7.5x10^{-3}$ Torr to $1.5x10^{-9}$ Torr. The cold cathode gauge/Penning gauge is an ionization gauge in which a high voltage discharge produces an electron beam that ionizes the gas in the chamber. The ions are then collected in an anode. The anode current will be proportional to the pressure of the chamber. A magnetic field is applied to increase the path of the charged particles and ionization current.

6.2.2 Differential pumping

Differential pumping is used to collect the unevaporated liquid from the chamber. The dry pump for pumping the liquid out can be seen in fig. 6.4. Figure

6.5 shows the collection system with an orifice of approx. 500μm diameter and 2cm length. This part reduces the back streaming of the liquid vapour to the chamber. This differential pumping arrangement is capable of maintaining four orders of magnitude difference in pressure between the collection system and the main chamber. The collection system is at a pressure of the order of 10^{-2} Torr whereas the chamber pressure can be as low as 10^{-6} Torr in the absence of the liquid jet. With the liquid jet introduced, the main chamber is found to work steadily at 10^{-3} Torr while the collection assembly is at 10^{-2} Torr.

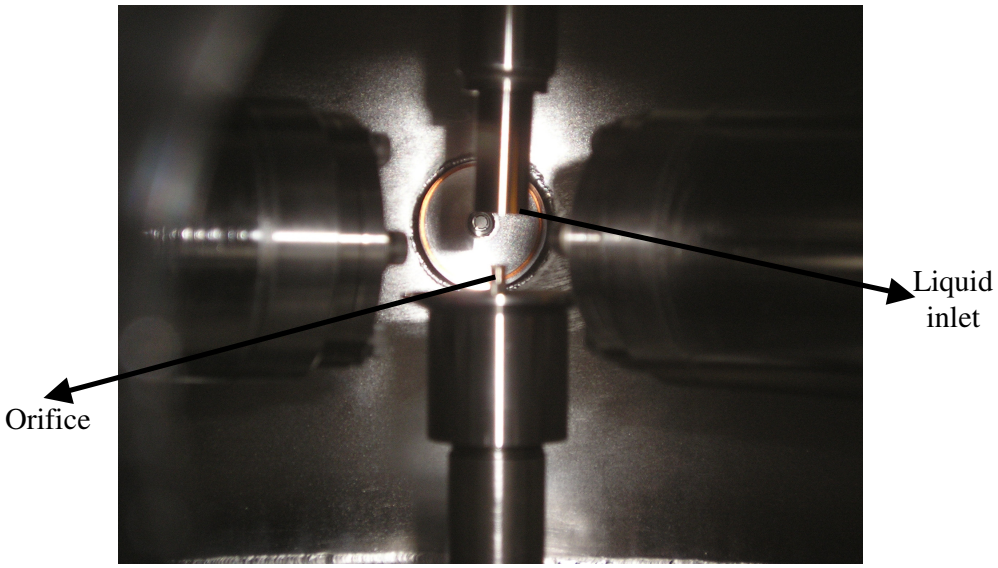

Figure 6.5: The liquid inlet and the collection assembly inside the chamber.

6.3 Production of the liquid microjet using a micro capillary

The liquid jet of approx. 10μm diameter is produced using a capillary tube of the same diameter. To produce a typical jet, initially ethanol is filled in a stainless steel container, which is shown in figure 6.6(a). The capillary is mounted at the tip of a stainless steel tube of length 50cm, and is inserted into the chamber through the top flange with a Wilson seal arrangement. This Wilson seal arrangement provides a vacuum compatible coupling by means of a rubber O-ring.

The liquid inlet mount is a bellow connected 6”’ flange through which the Wilson coupling of the capillary tube connection is inserted to the chamber. The liquid inlet mount has an x-y motion arrangement of 1cm in a plane parallel to the chamber central plane. This will allow flexible alignment of the liquid jet in the chamber in line with the collection assembly. The capillary tip is placed roughly 1 cm inside the SS inlet assembly to protect it from accidental destruction by the impact of the focused laser during beam alignment.

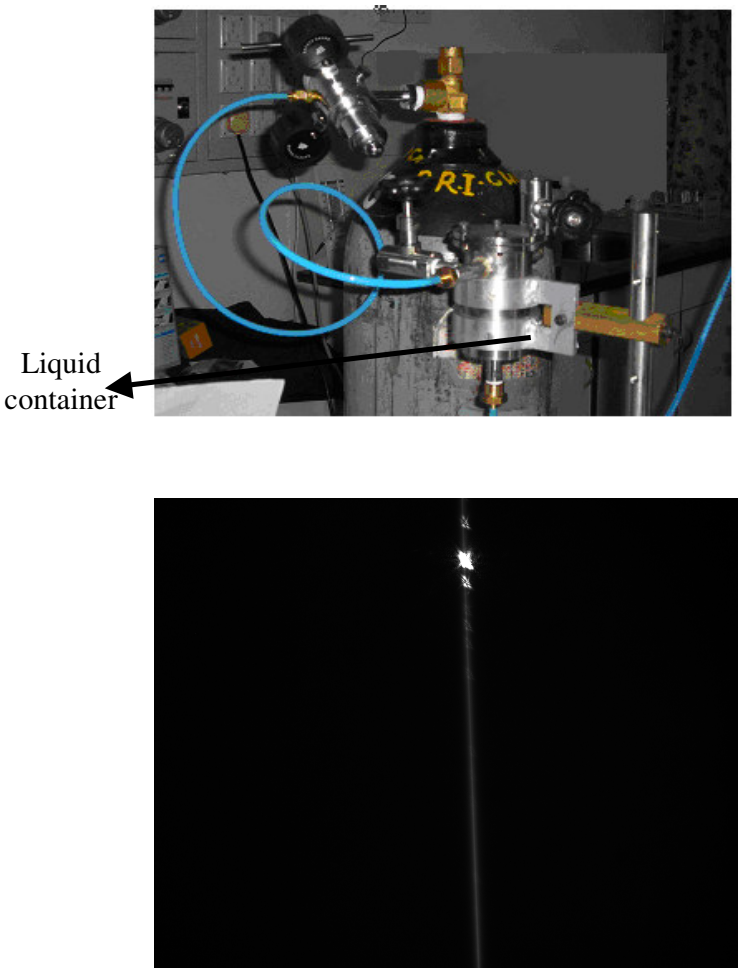

Figure 6.6: (a) Liquid inlet container and pressurizing cylinder. (b) liquid jet formed inside the chamber when an inlet pressure of 7bar is applied to the ethanol in the container. The bright spot is the 800nm, 100fs laser pulse focused onto the jet with a 10cm lens.

6.4 Solid State Detectors

For measuring high-energy radiations solid-state detectors are preferred over gas-filled detectors, as the former have material densities thousands of times higher than the latter. As the material density increases the number of interaction sites increases, leading to enhanced interaction probabilities so that the detector dimensions are considerably reduced. Solid state detectors from 'AMPTEK' (USA) have been chosen for our experimental set up.

6.4.1 X-Ray detector: Si-PIN

When radiation deposits energy in a semiconductor detector, an equal number of conduction electrons and holes are created within a few picoseconds along the radiation track. An electric field that is present throughout the detector active volume ensures that the electron-hole pairs experience an electrostatic force so that they drift to the corresponding electrodes, and get collected at the boundaries of the active medium, forming the signal. Even in the absence of ionizing radiation, semiconductors will show a finite conductivity and hence a leakage current, which may fluctuate enough to suppress signals originating from a true ionizing radiation, if the signal is weak. Hence to get a better signal to noise ratio, the leakage current should be a minimum. The depletion region of semiconductor diodes possess properties appropriate for a radiation detection medium. The electric field that exits at the depletion layer moves the newly generated electrons and holes to the *n*-type and *p*-type regions respectively.

Si-PIN detectors are used for detecting x-rays in the 1keV to 100keV regime. Even though the atomic number of silicon is as small as 14, the photoelectric absorption probability is more in the soft x-ray region below 20keV. In the silicon *p*-*i*-*n* diode configuration, a high resistivity *i*-region is introduced between the *p* and *n* non-injecting contacts on either surface. This configuration reduces the leakage current, thereby increasing the radiation detection probability. Apart from the minority charge carriers on the p and n regions, thermally induced

electron-hole pairs at the depletion layer also will contribute to the leakage current. Cooling of the semiconductor diode can reduce the thermally induced leakage current. The relatively small number of electron-hole pairs created by a low energy X-ray photon demands maximum reduction in the detector noise level. For this purpose the detectors are usually cooled thermo-electrically to temperatures like -30^0C .

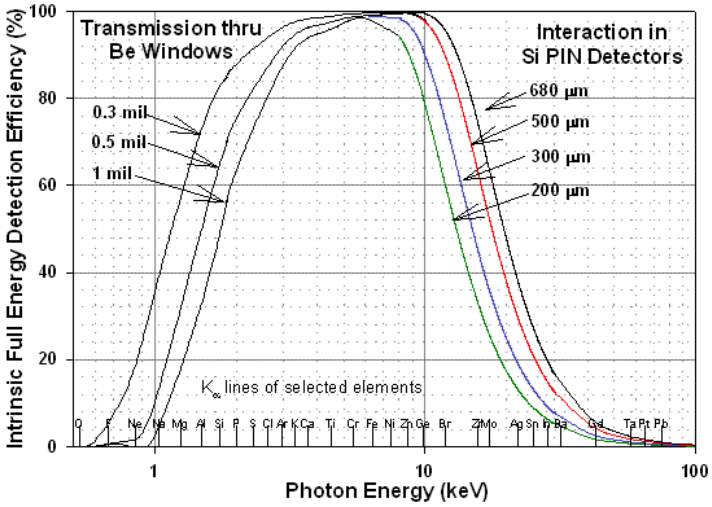

Figure 6.7: Intrinsic full energy detection efficiency of a Si-PIN detector. (From the instruction manual of Amptek XR 100CR Si-PIN detectors).

The Beryllium (Be) window on the detector XR100CR from Amptek filters low energy photons, thereby reducing the low energy background. As the thickness of the Be window increases, the low energy attenuation also increases as seen from figure 6.7. One mil corresponds to a thickness of 25µm of the Be window. The standard shaping time constant of the linear amplifier PX2CR is 12µs, and a higher energy resolution is obtained if 20µs shaping time is chosen. The detector XR100CR with 7mm^2 area and 300µm thickness having a Be window of 0.5mil thickness is capable of detecting the <1 to 30keV range with a pulse shaping time of 20µs. The other XR100CR detector with 5mm^2 area and 500µm thickness has a Be window of 1mil thickness, and it is capable of detection

in the 1.5-90keV range with a pulse shaping time of 12μs. The typical energy resolution of the former at 5.9keV is 180-190 eV and that of the latter is 185-205 eV. The Real Time Discriminator (RTD) provided with the amplifier PX2CR allows the gating of the shaped pulses so that only those pulses corresponding to 'good' X-ray events are allowed to be sent to the Multichannel Analyzer (MCA) for analysis. The internal threshold is set for 2keV, and if the detector is intended to detect below the 2keV limit, the RTD should be inactivated.

6.4.2. γ-Ray detector: NaI(Tl)

The operation of any radiation detector depends on the manner in which the radiation interacts with the material of the detector. The three important mechanisms of γ-ray interaction with matter that leads to their detection are the *photoelectric effect, Compton scattering and pair production*. As a result of these mechanisms the γ-ray will either completely disappear, or scatter to very large angles. In the photoelectric process the photon will be absorbed by the absorber atom, creating a photoelectron with a kinetic energy equivalent to the difference in energy between the incident photon and the binding energy of the electron. The predominant mode of interaction of x-rays and low energy γ-rays with matter is the photoelectric process. The process is enhanced for materials with higher atomic number and hence most of the γ-ray detectors are made of high-Z constituents. The probability per atom for Compton scattering depends on the number of electrons available and hence increases with the atomic number. If the γ-ray energy exceeds twice the rest mass energy of an electron (1.02 MeV), energetically, pair production is possible. In practice the probability of pair production is predominant only for very high-energy γ-rays in the 5-10 MeV range. The probability of pair production approximately scales as the square of the atomic number of the absorber. While photoelectric effect predominates the interaction of γ-rays with the detector material for γ-rays upto several hundreds of keV, Compton scattering is the predominant mechanism for γ-rays of intermediate energy.

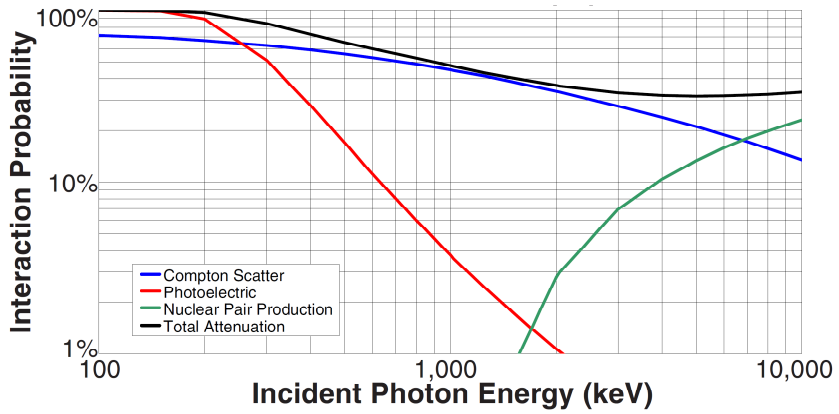

Figure 6.8: Computed interaction probabilities in the 30mm X 30mm Amptek make NaI(Tl) detector chosen for the present studies [from Amptek catalogue].

The interaction time or radiation stopping time in a typical radiation detector is a few nanoseconds for gaseous materials and a few picoseconds for solid materials. Hence for most practical situations energy deposition to the detector material is considered to be instantaneous. For a typical radiation detector, the net result of the interaction is the creation of a given amount of electric charge in the detector active volume and the electric signal is extracted from the detector material by applying an electric field within the detector. The time required to collect the charge is a few nanoseconds for semiconductor diode detectors, which depends on the mobility of the charge carriers inside the detector material and the distance traveled before reaching the collection electrodes.

The first solid medium used for γ-ray detection is NaI(Tl), and it continues to be in the frontier with its good light yield, linearity and the high atomic number of its iodine constituent. NaI(Tl) is a scintillator with excellent light yield that peaks at 415nm, and the dominant decay time of the scintillation pulse is 230ns. The conversion mechanism in a scintillator involves the conversion of the incident γ-ray to the corresponding optical emissions followed by the creation of photoelectrons. Thus a γ-ray detector should act as a conversion medium for the incident γ-rays to yield one or more fast electrons, and it must act as a

conventional radiation detector for the fast electrons thus generated. The relatively high atomic number of 53 of iodine ensures that photoelectric effect will be the dominant process in the NaI(Tl) detector. The photoelectric effect scales with the atomic number as $Z^{4.5}$. NaI(Tl) has a relatively high light output and smaller decay time, and better energy resolution compared to other scintillation detectors. It may be noted that the energy resolution is the poorest for scintillators compared to other radiation detectors. The finite energy resolution of a radiation detector is determined by the charge collection statistics, electronic noise, variation in the detector response over its active volume, and drift in the operation parameters over the course of the measurements. On the other hand for scintillation detectors, the fluctuations in the photo multiplier tube (PM tube) gain also is a determining factor of the resolution. Thus the energy resolution of scintillation detectors is basically limited by the photoelectron statistical fluctuations. The statistical fluctuations will be low if the number of photoelectrons produced per γ-ray event is large.

The Amptek GAMMA-8000 detector which we use for γ-ray detection is provided with a standard 30mm x 30mm NaI(Tl) scintillator crystal. The photo multiplier is a standard 30mm diameter tube. The scintillation crystal is housed in an anodized aluminium case of thickness 0.5mm, which reduces the background signals to the detector. The typical energy resolution is < 7.5% FWHM at 662keV and < 14% FWHM at 59.5 keV. A 20 turn potentiometer is provided for high voltage regulation in the 0-1500 V range.

6.4.3 Multichannel Analyzer (MCA)

A pulse height analyzer in a radiation detection system records the amplitude distribution of pulses produced by the detector. The linear amplifier shapes the pulse output from the preamplifier and increases the amplitude of the pulse to match it with the input of the multichannel analyzer. The operation of an MCA is based on the conversion of the pulse amplitude from a radiation detector to a corresponding digital number. An Analog to Digital Converter (ADC) is the

key component of an MCA. The ADCs designed to be used in an MCA differ from the standard ADCs in that they produce only a single output value for each analog pulse presented to their input, which is proportional to the peak amplitude of that pulse. The conventional ADC produces a continuous series of digital output values at a fixed clock frequency so that each part of the analog signal is converted to the corresponding digital number. The ADCs used with the MCA are named as *peak sensing ADCs*. The output of the ADC appears in a register that is used to address a digital memory that has addressable locations referred to as the channels into which the spectrum is subdivided. The number of memory locations (channels) is usually set as a power of 2. The bit depth of each memory location decides the maximum counting capacity of that memory location/channel. The commercially available memory locations usually have a maximum bit depth of 2^{32}, corresponding to a maximum capability of $4x\ 10^9$ counts per memory location. This means that the count in each channel will be saturated when the input pulse rate is higher than this counting value. Thus the basic function of an MCA is critically dependent on the ADC and the memory. The count of a given memory location is increased once the ADC output is comparable to the digitized amplitude corresponding to that memory location. When the ADC is digitizing the signal from the radiation detector, an input gate closes so that no other pulse is allowed at that time. The ADC is relatively slow, and if the counting rate of the detector is high, the gate will hence remain closed for many pulses so that the *dead time* will cause non-detection of these pulses. Hence for any absolute measurement of the number of pulses from the radiation detector, one has to take into account the correction for the detector dead time during which no signal is allowed to the ADC. Often the MCAs are provided with an option for Lower and Upper Level Discrimination of the input signal. This is to avoid any noise or background signal that happens to be either below the lower voltage level or above the higher voltage level. This will reduce the number of pulses to be processed by the ADC and hence reduce the fractional dead time below the 30% limit, above which the spectrum can be distorted. Thus to have significantly lesser dead time of the ADC, it is advisable to reduce the count rate of the radiation

presented to the detector and exclude noise including small and excessively large amplitude background events.

The full dynamic range of voltages available to the memory locations of the MCA for comparing and storing the ADC output can be set arbitrarily, depending on the total voltage range of the input signal from the radiation detector. Most of the ADCs designed for nuclear pulse processing are capable of handling the output of the linear amplifier and hence 0 to 10V is a common voltage span. The Amptek make MCA8000A which we use allows a dynamic range of 0-5V or 0-10V for the input pulse to its ADC. The voltage range is divided such that the highest channel number is assigned the 10V (for a 0-10V) and the lowest channel is assigned the lowest voltage value. Hence the resolution of the ADC will be at least as good as the largest conversion gain (or number of channels) at which it is used. For the Amptek MCA8000A used in the present studies, the highest resolution is attained when all the 16k channels are used. The overall dead time of the MCA is determined by the dead time of the ADC. The dead time basically consists of the processing time of the ADC and the memory storage time.

An ideal MCA will execute a perfectly linear conversion of the pulse height to the channel number. Thus a plot of the pulse height versus the channel number will be a straight line. In order to suppress high-count rates from very small noise pulses a zero offset is usually provided to the MCA so that a threshold amplitude is desired for the input pulse to be stored and displayed in the MCA. This threshold can be adjusted by the control panel or via software. Usually the signal from the detector is sent to a linear amplifier so that the signal amplitude is increased to match the set voltage levels of the ADC in the MCA. By increasing the gain of the linear amplifier, the amplitude of each signal is enhanced and the corresponding pulse height in the MCA will be increased, changing the slope of the calibration curve (Fig. 6.9). The same effect can also be obtained if the conversion gain of the ADC is adjusted. Assuming the MCA to be linear with the

pulse height, an energy calibration of the MCA that determines the energy scale of the pulse height distribution can be done by using radiation sources of known energy peaks. The slope and the y intercept of the straight line of calibration can be determined if one knows two of the energy lines, preferably those at the initial and final positions of the energy range of interest. A third energy value at the mid point will ensure linear calibration.

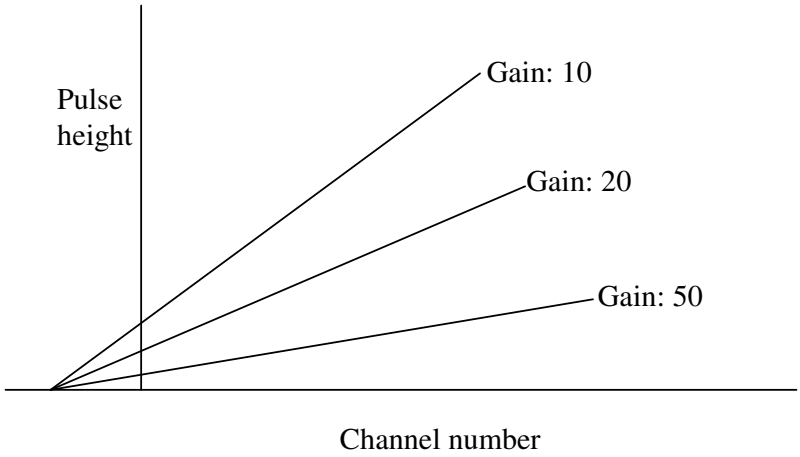

Figure 6.9 Schematic of MCA calibration plot for different gains of the linear amplifier [G.F. Knoll].

The Amptek pocket MCA8000A used in our detector system has software selectable number of channels/memory locations of 16k, 8k, 4k, 2k, 1k, 0.5k, and 0.25k. The resolution of the spectra is determined by the number of channels used for recording the spectra. The minimum pulse peaking time is 250ns and acquisition time of the analog pipeline is ≤ 2 μs. The ADC conversion time is ≤ 5 μs. There is a low level discriminator with software selectable threshold, in increment of one channel, up to half of the full range. The MCA has a nonvolatile memory having a 10-year data retention capacity. This capability is provided by a low power memory backed by an internal Lithium battery. The number of spectra that can be stored in the nonvolatile memory is given as 32k/ADC resolution, such that a maximum of 128 spectra can be stored in the memory at a time that

corresponds to an ADC resolution of 256 levels. The maximum counts per channel is 4.29 x 10^9. The serial interface has software selectable baud rates of 4.8kbps, 9.6kbps, 19.2kbps, 38.4kbps, 57.6kbps and 115.2 kbps.

6.5 Calibration of the Solid State detectors

In order to assign the energy of the peaks detected by the radiation detectors and stored in different channels of the MCA, one needs to calibrate the system with known radiation sources. For this, depending on whether the unknown spectra is expected to fall in the x-ray or in the γ-ray region, the appropriate detector is calibrated using standard radio active sources that have identifiable lines in the spectral region of interest.

6.5.1 X-Ray detectors

We used an Am^{241} source for the calibration of the x-ray detector, which has a strength of 0.1μCi. The calibrated spectra obtained using the Am^{241} radiation source are shown below. Figure 6.10a gives the spectra with the linear amplifier gain set to 0.5 and the ADC resolution to 2048. Figure 6.10b and 6.10c are the spectra obtained for gains of 0.8 and 0.9 respectively. It is seen that as the linear amplifier gain is increased, the spectra shifts towards the right. This is because the increased gain increases the amplitude of the pulse given to the ADC. Thus a pulse that would have been originally detected at a lower channel will now be detected at a higher channel, giving the option to discriminate the lower channels to suppress the low amplitude noise. Figure 6.10d & 6.10e are the calibration spectra with the ADC resolution increased to 4096 channels. The characteristic lines at 13.9, 17.8, 20.8, 26.35 and 59.5keV are identified from the spectra.

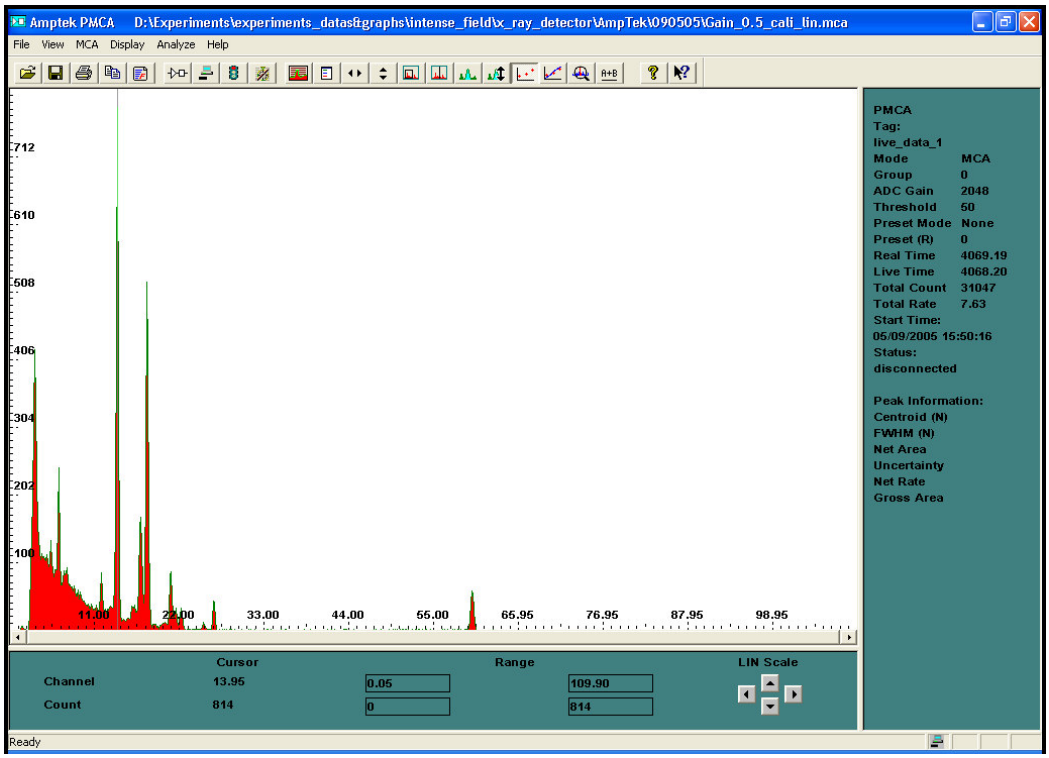
Amptek PMCA D:\Experiments\experiments_datas&graphs\intense_field\x_ray_detector\AmpTek\090505\Gain_0.5_cali_lin.mca
File View MCA Display Analyze Help
712
610
508
406
304
202
100
11.00
22.00
33.00
44.00
55.00
65.95
76.95
87.95
98.95
PMCA
Tag:
live_data_1
Mode MCA
Group 0
ADC Gain 2048
Threshold 50
Preset Mode None
Preset (R) 0
Real Time 4069.19
Live Time 4068.20
Total Count 31047
Total Rate 7.63
Start Time:
05/09/2005 15:50:16
Status:
disconnected
Peak Information:
Centroid (N)
FWHM (N)
Net Area
Uncertainty
Net Rate
Gross Area
Cursor
Range
LIN Scale
Channel 13.95 0.05 109.90
Count 814 0 814
Ready

(a)

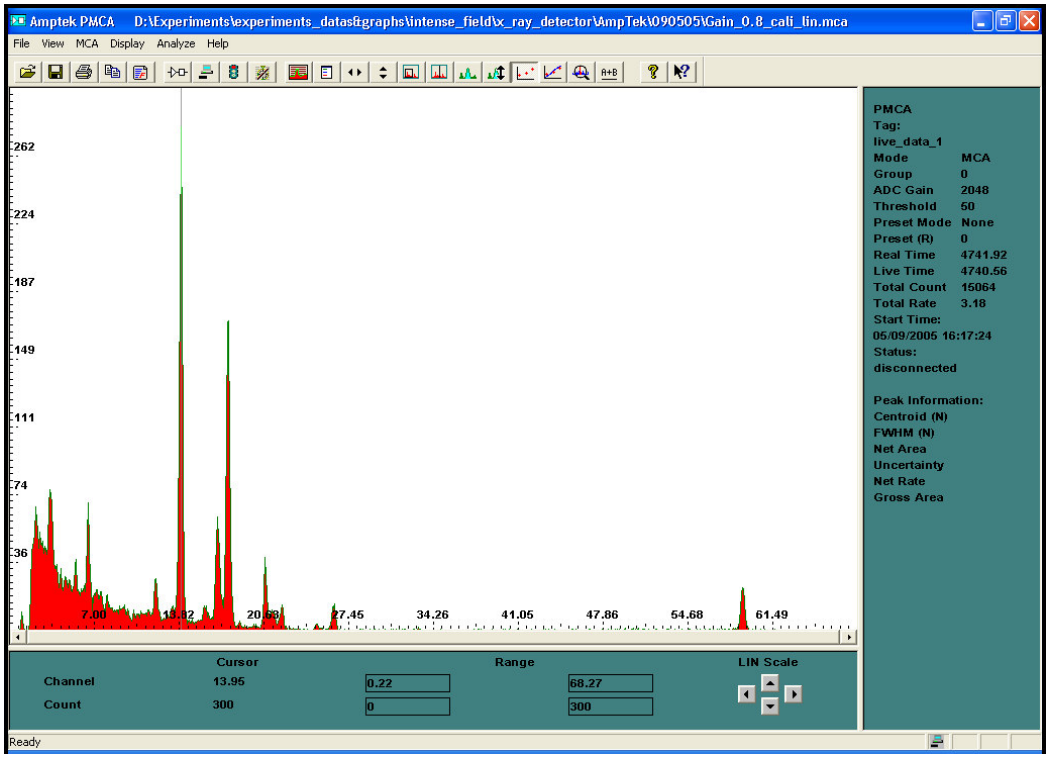
Amptek PMCA D:\Experiments\experiments_datas&graphs\intense_field\x_ray_detector\AmpTek\090505\Gain_0.8_cali_lin.mca
File View MCA Display Analyze Help
262
224
187
149
111
74
36
7.00
13.82
20.63
27.45
34.26
41.05
47.86
54.68
61.49
PMCA
Tag:
live_data_1
Mode MCA
Group 0
ADC Gain 2048
Threshold 50
Preset Mode None
Preset (R) 0
Real Time 4741.92
Live Time 4740.56
Total Count 15064
Total Rate 3.18
Start Time:
05/09/2005 16:17:24
Status:
disconnected
Peak Information:
Centroid (N)
FWHM (N)
Net Area
Uncertainty
Net Rate
Gross Area
Cursor
Range
LIN Scale
Channel 13.95 0.22 68.27
Count 300 0 300
Ready

(b)

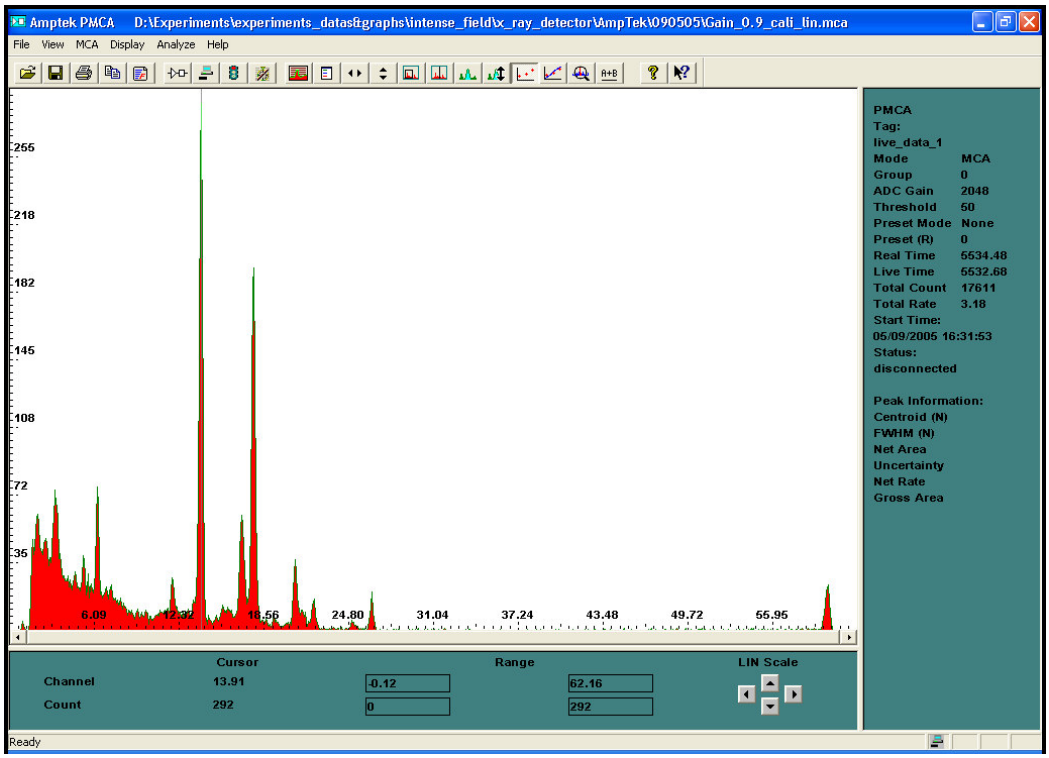
Amptek PMCA D:\Experiments\experiments_datas&graphs\intense_field\x_ray_detector\AmpTek\090505\Gain_0.9_cali_lin.mca
File View MCA Display Analyze Help
255
218
182
145
108
72
35
6.09
12.32
18.56
24.80
31.04
37.24
43.48
49.72
55.95
PMCA
Tag:
live_data_1
Mode MCA
Group 0
ADC Gain 2048
Threshold 50
Preset Mode None
Preset (R) 0
Real Time 5534.48
Live Time 5532.68
Total Count 17611
Total Rate 3.18
Start Time:
05/09/2005 16:31:53
Status:
disconnected
Peak Information:
Centroid (N)
FWHM (N)
Net Area
Uncertainty
Net Rate
Gross Area
Cursor
Range
LIN Scale
Channel 13.91 -0.12 62.16
Count 292 0 292
Ready

(c)

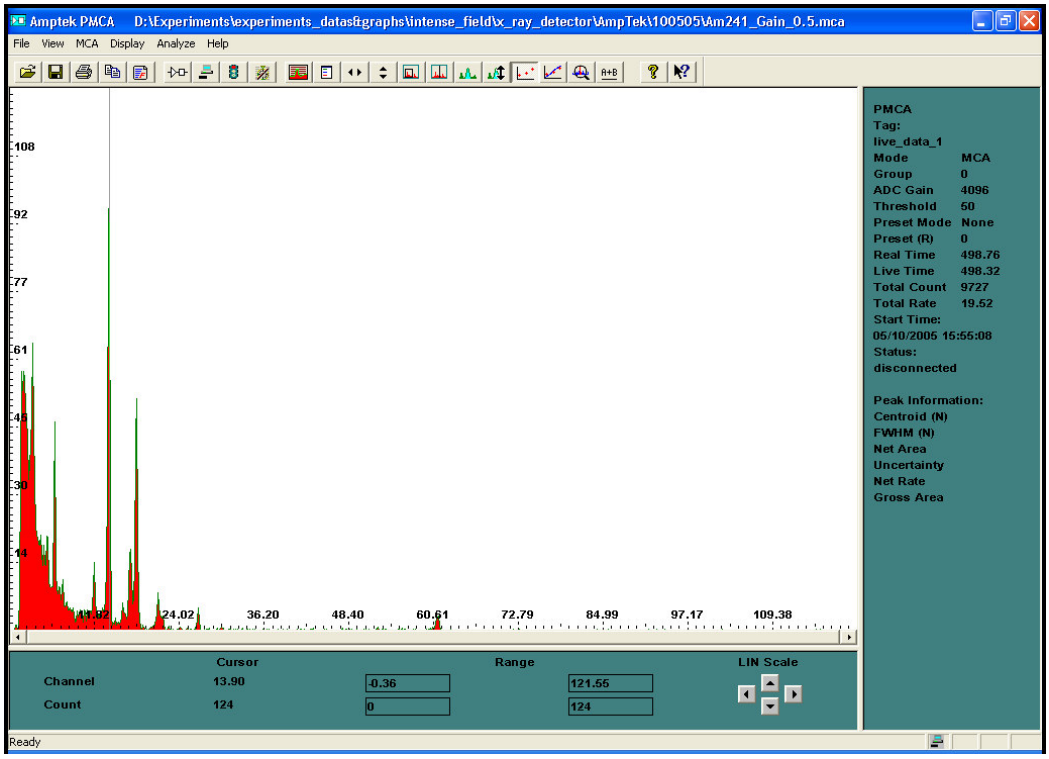
Amptek PMCA D:\Experiments\experiments_datas&graphs\intense_field\x_ray_detector\AmpTek\100505\Am241_Gain_0.5.mca
File View MCA Display Analyze Help
108
92
77
61
46
30
14
24.02
36.20
48.40
60.61
72.79
84.99
97.17
109.38
PMCA
Tag:
live_data_1
Mode MCA
Group 0
ADC Gain 4096
Threshold 50
Preset Mode None
Preset (R) 0
Real Time 498.76
Live Time 498.32
Total Count 9727
Total Rate 19.52
Start Time:
05/10/2005 15:55:08
Status:
disconnected
Peak Information:
Centroid (N)
FWHM (N)
Net Area
Uncertainty
Net Rate
Gross Area
Cursor
Range
LIN Scale
Channel 13.90 -0.36 121.55
Count 124 0 124
Ready

(d)

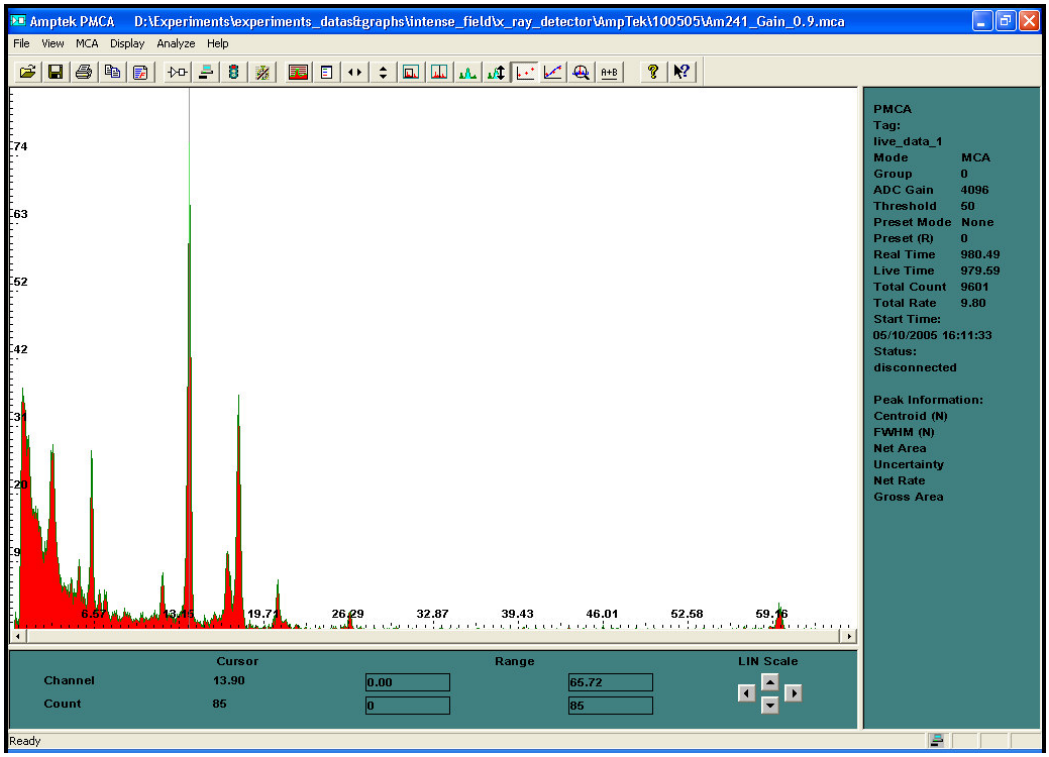

(e)

Figure 6.10a-e: Calibration of the x-ray detector system, which uses the XR100CR detector head using an Am^{241} source.

6.5.2 γ-Ray detectors

Two of the widely used γ-ray calibration sources are Co^{60} and Cs^{137}.

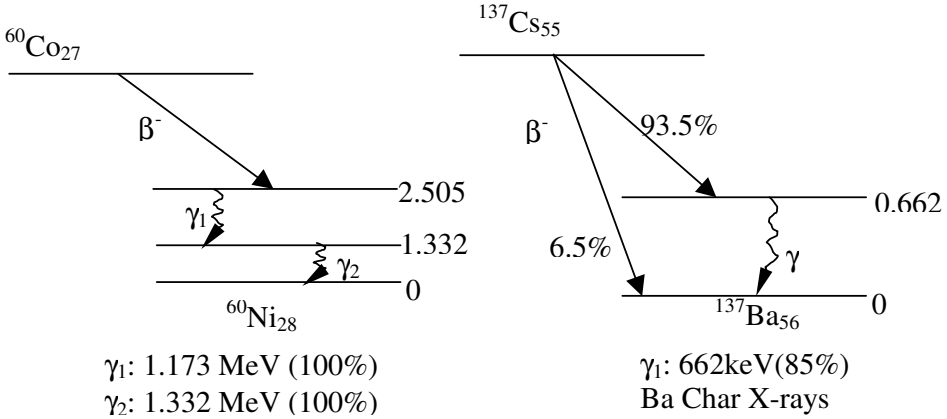

Fig. 6.11: Decay scheme for the γ-Ray reference sources Co^{60} and Cs^{137}. Only the major transitions are shown.

The nuclear decay schemes of these are illustrated in fig. 6.11 [G.F.Knoll]. In each case a form of β-decay leads to the population of the excited state in the daughter nucleus. De-excitation of the daughter nucleus takes place through the emission of a γ-ray photon whose energy is equal to the difference in energy between the initial and final nuclear states of the daughter nucleus. The γ-ray thus appears with a half-life characteristic of the parent β-decay but with an energy that reflects the energy level structure of the daughter nucleus. Thus the 'C^{60} γ-rays' decrease in intensity with the 5.26-year half-life characteristic of C^{60} even though their actual origin is from transitions in the daughter N^{60} nucleus. Since nuclear states have well defined energies, the γ-rays emitted are nearly monoenergetic and the inherent line width of the photon energy distribution is small compared to the energy resolution of the detectors used. Hence the detector response is indicative of its own limiting resolution rather than any variation in the incident γ-ray energy. The Cs^{137} source we used to calibrate the γ-ray detector has a strength 3.3mCi and the Co^{60} source has a strength of of 2.4mCi. The Calibration of the γ-ray detector system with C^{137} is shown in fig 6.12.

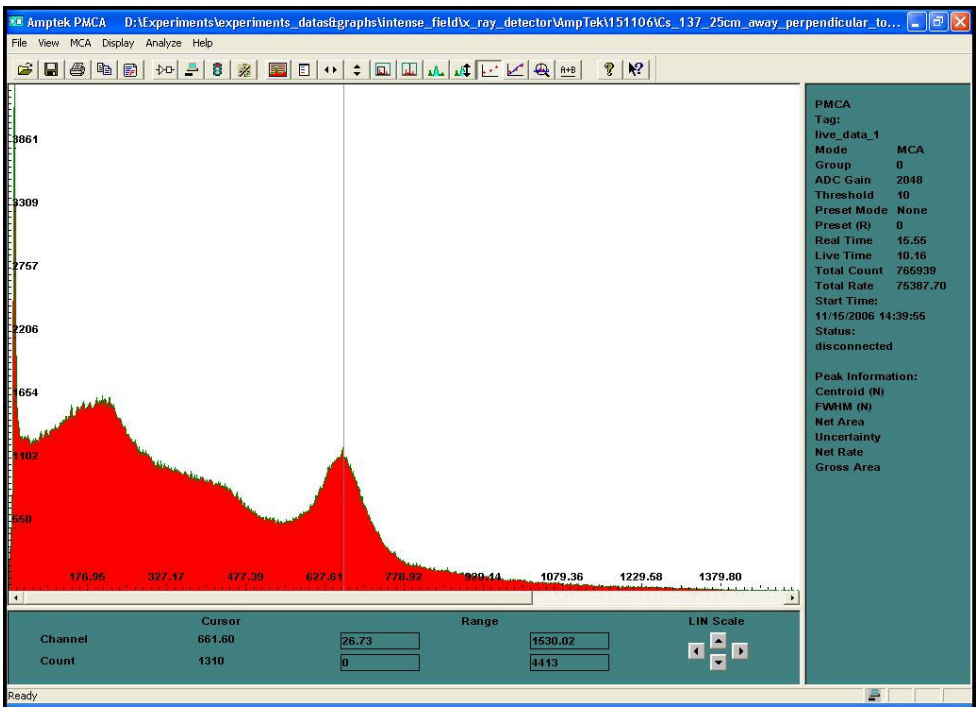

Figure 6.12: Calibration of the NaI(Tl) detector system using Cs^{137} .

6.6 Time gating and synchronization of the NaI (Tl) detector

The NaI(Tl) detector is susceptible to background radiation coming from ambient radioactive elements. To improve the signal to noise ratio, we applied a time gate to the MCA. MCA gating can be applied also to attain a data accumulation time shorter than one second or for non-integer accumulation times. There is a provision to apply a time window of variable width (1μs to 1s) to the gate 2 of the MCA. This is an active LOW TTL compatible logic gate. When this input is LOW, the analog input pulses are gated off. The data is acquired only in the time window when the TTL input is HIGH, which is determined by the set time window. The key parameters in the MCA8000A data acquisition configuration are the low level threshold and the data acquisition time. The low level threshold is digitally set and stored in the nonvolatile memory. The acquisition time can be preset as either live or real, since the MCA8000A has both real and live time clocks. The live time clock adjusts for deadtime by turning off the clock whenever (a) the input signal exceeds the low level threshold, (b) the analog pipeline is holding a pulse to be processed by the ADC, or (c) one or both of the MCA gates are active. A function generator is used for this time gating in synchronization with the laser firing. The function generator used is SRS DS345 (Stanford Research Systems). It has a rear-panel TRIGGER input, which is TTL compatible. A BURST/SWEEP output from the function generator is triggered in accordance with this TTL signal. The triggering can be set to either POS IN or NEG IN edge trigger. The Q-switch SYNC output of the Nd:YAG laser, which is the pumping laser for the femtosecond amplifier used in these experiments, gives a pulse synchronous with the laser output. The pulse width is 2.5ms and the pulse height is 4.88V when connected to the 1MΩ input of an oscilloscope. The pulse repetition rate is 10Hz, which is the same as the repetition rate of the laser. These pulses are used to trigger the BURST MODE of the function generator, so that the DS345 generates bursts of one of its periodic output functions. The frequency of the output function is limited to 1 MHz for sine and square waves, and 100 kHz for triangles and ramps. There is no frequency limit for the output function ARB ('arbitrary'). When a trigger signal is received, the DS345 initiates a burst starting

at a specific point (phase) in the output waveform, outputs the exact number of programmed waveform cycles, and then stops. Simultaneously, the rear-panel TRIGGER OUTPUT generates a TTL compatible signal that goes high when the burst is triggered and low when the burst is complete. This signal is used to synchronize the MCA (or any external equipment) to the burst. In order to generate the desired pulses for time-gating the MCA, the burst time is set equal to the required pulse width. The time for a burst is easily computed from the following formulae:

Burst Time = Burst Count/Frequency (for sine, square, triangle and ramp waveforms)

Burst Time = (Burst Count x # Waveform Points)/Sampling Frequency
(for ARB waveforms)

As an example, in order to get a time gate of 20μs, the burst time in the function generator is set to 20μs by setting the burst count to 1 and the frequency of the sine wave (it can also be square/triangle/ramp) to 50kHz. The TTL output of the DS345 rear panel gives a TTL compatible pulse with a HIGH of 20μs duration, which is fed to gate 2 of the MCA, which enables a data acquisition window of 20μs every cycle, at the rate of 10Hz (which is the trigger frequency). The burst time can be altered either by changing the burst count or the signal frequency. The data acquisition rate can be changed by adjusting the trigger rate. Triggering using the Nd:YAG Q-switch, automatically synchronizes the X-Ray generation process and the detection process. This ensures a synchronized, background free detection of the hard X-Ray produced in the laser-plasma interaction.

The reduction in background with time gating applied to the MCA for the NaI(Tl) detector is shown in figure 6.13. A low level discrimination is applied at channel number 10. The number of channels is set to 1024 and the real time taken for recording the spectrum is 50sec. The time gate and the trigger repetition rate determine the live time of observation. The 1s time gate data is taken for a duration of 17.5sec only. The counts shown in the graph is truncated for higher

counts. This shows the effectiveness of time gating in the data acquisition. From Figure 6.13 it is clear that as the width of the time gate is decreased the counts also decreases.

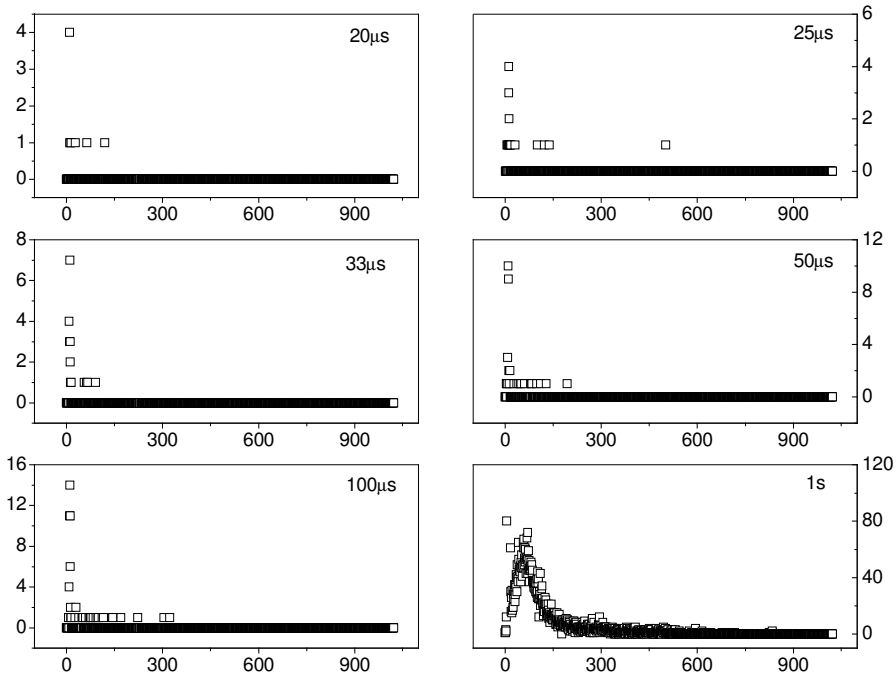

Figure 6.13: Illustration of the effectiveness of gating the MCA for reduction of background. No source is present. Total number of channels is set to 1024 and the low level threshold is set to channel 10.

In conclusion, we have completed the design and implementation of an experimental setup for the study of the interaction of intense laser pulses with a liquid microjet in vacuum. Fabrication details of the high vacuum chamber with differential pumping are given. This chamber is capable of handling an injected liquid load of a few micro liters per second while sustaining a working pressure of 10^{-3} Torr. Introducing liquid into a vacuum chamber and maintaining a low vacuum is technically challenging, and we have attained this goal successfully. If cryopumping is applied in the present system, vacuum will improve substantially.

With some modifications, this system will be capable of studying plasma generated in liquid droplets. Details of the x-ray and γ-ray detectors to be used for recording the plasma emission, and their synchronization and calibration, are also explained.

Conclusions and Future Prospects

This thesis contains studies of nonlinear light transmission through noble metal nanoparticles, nonreciprocal transmission of laser pulses through nonlinear media, and spectral features of femtosecond laser induced plasma from a thin liquid jet. The design and fabrication of an experimental set up to study high energy photons emitted by an intense field plasma in vacuum also is included.

We have investigated the nonlinear transmission of light through Au, Ag and Au:Ag nanoparticle systems, of average sizes ranging from 1 nm to 60 nm, in the nanosecond as well as ultrafast (femtosecond) time scales. Experimental and numerical studies reveal that both absorption saturation and optical limiting behaviour are exhibited by these metal nanoparticles depending on their size, concentration and the input laser fluence. The samples except those of 1 nm size show a strong surface plasmon resonance in the visible region. Our studies show that these materials are suitable candidates for saturable absorption and optical limiting applications.

From numerical simulations we have shown that nonreciprocal optical transmission can be achieved in a tandem assembly of a saturable absorber and reverse saturable absorber, which can be used for optical diode applications. Experimental confirmation also is given to validate the simulations. Unlike some of the currently suggested optical diodes based on materials like photonic crystals, this device will work for all light polarizations, has no phase-matching restrictions, and can be fabricated from a large number of different nonlinear media. Another advantage is that saturable and reverse saturable materials are available in different forms (solution, polymer films, quantum dots etc.) suitable for a wide range of potential applications.

We have studied the spectral features of second harmonic and incoherent emission from plasma in a planar water jet induced by ultrafast laser pulses of 100 femtoseconds duration. The experiments are performed in the intensity range of 10^{14} W/cm^2 to 10^{15} W/cm^2, for normal incidence as well as oblique incidence. For normal incidence we observed H_α and H_β recombination lines along with the continuum that accompanies recombination. The continuum and recombination lines are unpolarized. When the input laser intensity exceeds $2x10^{15}$ W/cm^2 significant ionization occurs in the medium and a spectral blue shift is observed for the input laser pulse that is scattered from the plasma. This is due to the rapid refractive index variation seen by the laser pulse once the ionization becomes significant. For oblique incidence at an angle of 45^0 we observed second harmonic emission of the incident laser pulse, which is a maximum when the input is *p*-polarized. Here the electron plasma waves which are excited at the critical density layer via resonance absorption mechanism non-linearly couple with the oscillatory velocity of the plasma electrons, resulting in an ac electronic current in the plasma that eventually radiates the second harmonic of the incident light. Our interaction intensity regime of 10^{15} W/cm^2 is one or two orders of magnitude less than that of the previously reported studies. The relative amplitudes of the observed SH and incoherent visible radiation suggests that the intensity level is below the plasma wave breaking regime.

We have designed and fabricated an experimental setup for the study of intense laser induced plasma from a liquid microjet in vacuum. The vacuum chamber has a volume of 300 lt and it can be evacuated to a pressure of 10^{-6} Torr. It is equipped with suitable detectors for recording the visible, X-ray and γ-ray emissions. With some modifications, it is possible to use liquid droplets as targets in this system.

It would be interesting to investigate in more detail, the temporal dynamics of nonlinear transmission in metal nanoparticles. Our measurements have shown that the timescales involved can be very fast, in the order of a few picoseconds.

Fast response is one of the crucial aspects in photonic applications like optical limiting. Similarly, one could also study the energetic electrons and ions present in a femtosecond plasma, to obtain a deeper insight to the various processes happening in the laser-plasma interaction. Another interesting aspect of the intense field plasma is the generation of very large magnetic fields. It is hoped that these studies will be taken up in the near future making use of the experimental setup which is now put in place.

Bibliography

1) Agostini P., Fabre, F., mainfray, G., and Rahman,N.K., Phys.Rev.Lett., **42**, 1127 (1979).
2) Agostini P. and Petite G., Cont. Phys. **29,** 57 (1988).
3) Alvarez, M. M., Khoury, J. T., Schaaff, T. G., Shafigullin, M. N., Vezmar I., and Whetten, R. L., J. Phys. Chem. B, **101,** 3706 (1997).
4) Anand, M., Gibbon, P., and Krishnamurthy, M., Opt. Express, 14, 5502 (2006).
5) Andreev, A. A., Platonov, K. Yu., Gauthier, J.C., Phys. Rev. E, **58**, 2424 (1998) .
6) Batani D., Joachain, C. J., Martellucci, S., and Chester, A. N., Atoms, Solids and Plasmas in Super-intense laser fields, Kluwer Academic/Plenum Publishers, New York, 2001.
7) Bloembergen, N., Rev. Mod. Phys., 71, S283 (1999).
8) Boyd, R. W., Nonlinear Optics, Academic Press, San Diego, 2003.
9) Brabec T., and Kraus F., Rev. Mod. Phys., Vol.**72**, No.2, 545(2000).
10) Brunel, F., Phys. Rev. Lett., 59, 52 (1987).
11) Bucksbaum, P.H., Freeman, R.R., Bashkansky, M. and McIlrath, T. J., J. Opt. Soc. Am. B, **4**, 760 (1987).
12) Champaret, J. P., LeBlanc, C., Cheriaux, G., Curley, P., Darpentigny, C., and Rousseau, P., Opt. Lett., **21**, 1921 (1996).
13) Chelkowski, S., A. Conjusteau, T. Zuo, and A. D. Bandrauk, Phys. Rev. A, 54, 3235 (1996).
14) Chu, S. I., and Yin, R. Y., J. Opt. Soc. Am. B, **4**, 720 (1987).
15) Clark, E, L., Krushelnik, K., Davies, J. R., Zepf, M., Tatarakis, M., Beg, F. N., Machacek, A., Norreys, P. A., Santala, M. I. K., Watts, I. , and Dangor A. E., Phys. Rev. Lett., **84**, 670 (2000).
16) Cook, C.E., Proc. IRE, **48**, 310 (1960).
17) Cormier, E., and Lambropoulos, P., Eur. Phys. J. D., **2**, 15 (1998).

18) Couris, S., Koudoumas, E., Ruth, A. A., Leach, S., J. Phys. B, 28, 4537 (1995).

19) Curley, P. F., Spielmann, Ch., Brabec, T., Krausz, F., Wintner, E., and Schmidt, A. J., Opt. Lett., **18**, 54 (1993).

20) Deng, Z., and Eberly, J., J. Opt. Soc. Am. B, **2**, 486 (1985).

21) Dabbousi, B. O., Rodriguez-Viejo, J., Mikulec, F. V., Heine, J. R., Mattoussi, H., Ober, R., Jensen, K. F., and Bawendi, M. G., J. Phys. Chem. B, **101**, 9463 (1997).

22) Danek, P. S. M., Jensen, K. F., Murray, C. B., and Bawendi, M. G., Chem. Mater., 8, 173 (1996).

23) DiDomenico, M., J. Appl. Phys., 35, 2870 (1964).

24) Diels, J.C., and Rudolph, W., Ultrashort laser pulse phenomena, Academic Press, San Diego, 1996.

25) Eberly, J.H., and Lambropoulos, P., Multiphoton Processes, John Wiley & Sons, New York, 1978.

26) Eesley, G. L., Phys. Rev. B, 33, 2144 (1986).

27) Eickmans, J. H., Hsieh, W. F., and Chang, R. K., Opt. Lett. **12**, 22(1987).

28) Eidmann , K., and Sigel, R., Phys. Rev. Lett., 34, 799 (1975).

29) Ell, R., Morgner, U., and Kartner, F. X., Fujimoto, J. G., and Ippen, E. P., Scheuer, V., Angelow, G., and Tschudi, T., Lederer, M. J., Boiko, A., and Luther-Davies, B., Opt. Lett., 26, 373 (2001).

30) Engers, T., Fendel, W., Schuler, H., Schulz, H., and Linde, D. von der, Phys. Rev. A, **43**, 4564 (1991).

31) Fabre, F., Agostini, P., and Petite, G., Phys. Rev. A, **27**, 1682 (1983).

32) Faisal, F.H.M., Theory of Mutiphoton processes, Plenum Press, New York, 1987.

33) Favre, C., Boutou, V., Hill, S. C., Zimmer, W., Krenz, M., Lambrecht, H., Yu, J., Chang, R. K., Woeste, L., and Wolf, J. P., Phys. Rev. Lett. **89**, 035002 (2002).

34) Federov M.V., Atomic and free electrons in a strong light field, World scientific, Singapore, 1997.

35) Feit, M. D., Komashko, A. M., and Rubenchik, A. M., Appl. Phys. A, **79**, 1657 (2004).

36) Feldheim D. L., and Colby A. Foss Jr., Metal nanoparticles: Synthesis, Characterization, and Applications, Marcel Dekker, New York, 2002.

37) Feng, Q., Moloney, J. V., Newell, A.C., Wright, E. M., Cook, Kennedy, P. K., Hammer, D. X., Rockwell, B. A., and Thompson, C. R., IEEE J. Quantum Electron. **33**, 127(1997).

38) Fork, R.L., Brito Cruz, C.H., Becker, P.C., and Shank C.V., Opt. Lett., **12**, 483 (1987).

39) Francois, L., Mostafayi, M., Belloni, J., Delouis, J-F, Delaire, J., Feneyrou, P., J. Phys. Chem. B, 104, 6133 (2000).

40) Gaponov, A. V., and Miller, M. A., Sov. Phys. JETP, **7**, 168 (1958).

41) Gizzi, L. A., Giulietti, D., and Giulietti, A., Audebert, P., Bastiani, S., Geindre, J.P., and Mysyrowicz, A., Phys. Rev. Lett., **76**, 2278 (1996).

42) Griem, H. R., Principles of plasma spectroscopy, Cambridge university press, Cambridge, 1997.

43) Grimes, M.K., Rundquist, A. R., Lee, Y. S., and Downer, M. C., Phys. Rev. Lett., **82**, 4010 (1999).

44) Hache, F., Ricard, D., Flytzanis, C., Kreibig, U., Appl. Phys. A, **47**, 347 (1988).

45) Hansen, C. T., Wilks, S. C., and Young, P. E., Phys. Rev. Lett., **83**, 5019(1999).

46) Hargrove, L. E., Fork, R. L., and Pollack, M. A., Appl. Phys. Lett., **5**, 4 (1964).

47) Hwang, J., Song, M. H., Park, B., Nishimura, S., Toyooka, T., Wu, J. W., Takanishi, Y., Ishikawa, K., and Takezoe, H., Nature Materials **4**, 383 (2005).

48) Ispasoiu, R. G., Balogh, L., Varnayski, O. P., Tomalia, D. A., Goodson III, T., J. Am. Chem. Soc., 122, 11005 (2000).

49) Jung, I.D., Kartner, F.X., Matuschek, N., Sutter, D. H., Morier-Genoud, F., Zhang, G., and Keller, U., Scheuer, V., Tilsch, M., and Tschudi, T., Opt. Lett., **22**, 1009 (1997).

50) Kaiser, W., and Garrett, C.G.B., Phys. Rev. Lett., **7**, 229 (1961).

51) Kamat, P. V., Flumiani, M., Hartland, G. V., J. Phys. Chem. B, **102**, 3123 (1998).

52) Katia Gallo, JOSAB 16, 267 (1999).

53) Kato, S., Kawakami, R., and Mima, K., Phys. Rev. A, **43**, 5560 (1991).

54) Keitel, C. H., Contemporary Physics, 42, 353 (2001).

55) Keldysh, L. V., Sov. Phys. JETP **20**, 1307 (1965).

56) Keller, U., 'tHooft, G.W., Knox, W.H., and Cunningham, J. E., Opt. Lett., **16**, 1022 (1991).

57) Keller, U., Nature, **424**, 831 (2003).

58) Kennedy, P. K., IEEE J. Quantum. Electron. 31, 2241(1995).

59) Kennedy, P.K., Boppart, S. A., Hammer, D. X., Rockwell, B. A., Noojin, G. D., and Roach, W. P., IEEE J. Quant. Electron. **31**, 2250 (1995).

60) Kennedy, P. K., Hammer, D. X., and Rockwell, B. A., Prog. Quant. Electr. **21**,155(1997).

61) Kim, K. Y., Alexeev, I., Antonsen, T. M., Gupta, A., Kumarappan, V., and Milchberg, H. M., Phys. Rev. A., **71**, 011201 (2005).

62) Kmetec, J., Macklin, J.J., and Young, J.F., Opt. Lett., **16**, 1001(1991).

63) Knoll, G. F., Radiation Detection and Measurement, Third Edn., John Wiley & Sons Inc., New York, 2000.

64) Krause, J. F., Schafer, K. J., and Kulander, K. C., Phys. Rev. A, **45**, 4998 (1992).

65) Kreibig, U., and Volmer, M., Optical Properties of Metal Clusters, Springer Verlag, Berlin, 1995.

66) Krishan, V., Astrophysical plasmas and fluids, Kluwer academic publishers, Dordrecht, 1999.

67) Kruer, W. L., The Physics of laser plasma interactions, Addison-Wesley Publishing Company, California, 1988.

68) Kyrala, G. A., J. Opt. Soc. Am. B, **4**, 731 (1987).

69) Landau, L.D., Lifshitz, E.M., Electrodynamics of continuous media, Pergamon Press, Oxford, 1984.

70) Ledingham, K. W. D., McKenna, P., Singhal, R. P., Science, **300**, 1107 (2003).

71) Linde, Dietrich von der, Schulz, H., Engers, T., and Schuler, H., IEEE J. Quantum Electron., **28**, 2388, 1992.

72) Link, S., El Sayed, M. A., Schaaff, T. G., Whetten, R. L., Chem. Phys. Lett., 356, 240 (2002).

73) Logunov, S. L., Ahmadi, T. S., El-Sayed, M. A., Khoury, J. T., Whetten, R. L., J. Phys. Chem. B, **101**, 3713 (1997).

74) Lompre, L.A., L'Huillier, A., Mainfray, G., and Manus, C., J. Opt. Soc. Am. B, **2**, 1906 (1985).

75) Maine, P., Strickland, D., Bado, P., Pessot, M., and Mourou, G., IEEE J. Quantum E.ectron., **24**, 398 (1988).

76) Mainfray, G., and Manus, C., Rep. Prog. Phys., **54**, 1333 (1991).

77) Maltesev, A., and Ditmire, T., Phys. Rev. Lett., **90**, 053002 (2003).

78) Michael W. Feise, Ilya V. Shadrivov, and Yuri S. Kivshar, PRE **71**, 037602 (2005).

79) Milchberg, H. M., and Freeman, R. R., Phys. Rev. A, **41**, 2211(1990).

80) Milonni, P.W., Eberly, J.H., Lasers, John Wiley & Sons, New York, 1988.

81) Mingaleev, S. F., and Kivshar, Y. S., J.Opt.Soc.Am.B. **19**, 2241 (2002).

82) Mishra, S. R., Rawat, H. S., Mehendale, S. C., Rustagi, K. C., Sood, A. K., Bandopadhyay, R., Govindaraj, A., Rao, C. N. R., Chem. Phys. Lett., **317**, 510 (2000).

83) Moulton, P. F., J. Opt. Soc. Am. B, **3**, 125 (1986).

84) Mujumdar, S., and Ramachandran, H., Opt. Lett. **26**, 929 (2001).

85) Nahen, K., and Vogel, A., IEEE J. Selected topics in Quant. Electron. **2**, 861(1996).

86) Nair A.S. , Suryanarayanan, V., Pradeep, T., Thomas, J., Anija, M., and Philip, R., Materials Science and Engineering B 117 (2005) 173.

87) Noack, J., and Vogel, A., IEEE J. Quant. Electron. **35**, 1156 (1999).

88) Patterson, F. G., and Perry, M. D., J. Opt. Soc. Am. B, **8**, 2384 (1991).

89) Penetrante, B. M., Bardsley, J. N., Wood, W. M., Siders, C. W., and Downer, M. C., J. Opt. Soc. Am. B, **9**, 2032 (1992).

90) Perry M. D., Patterson, F. G., Weston, J., Opt. Lett., **15**, 381 (1990).

91) Perry, M.D., and Mourou G., Science, 264, 917 (1994).

92) Pert, G. J., Phys. Rev. E, **51**, 4778 (1995).

93) Pessot, M., Maine, P., Mourou G., Opt. Commun., 62, 419 (1987).

94) Pessot, M., Squier, J., Bado, P., Mourou, G., Harter, D., IEEE J. Quantum Electron., **25**, 61, (1989).

95) Philip, R., Ravindrakumar, G., Mathur, P., Ghosh, S., Chem. Phys. Lett., **313**, 719 (1999).

96) Philip, R., Ravindrakumar, G., Mathur, P., Ghosh, S., Opt. Commun., **178**, 469 (2000).

97) Philip, R., Ravindrakumar, G., Sandhyarani, N., and Pradeep, T., Phys. Rev. B, **62**, 13160 (2001).

98) Philip, R., Mujumdar, S., Ramachandran, H., Ravindrakumar, G., Sandhyarani, N., Pradeep, T., Nonlinear Opt., 27, 357 (2001).

99) Philip, R., Anija, M., Yelleswarapu, C.S., Rao, D.V.G.L.N., Optics Letters

100) Pradeep, T., Nano: The Essentials, Tata McGraw-Hill, New Delhi, 2007.

101) Protopapas, M., Keitel, C. H., and Knight, P. L., Rep. Prog. Phys., **60**, 389 (1997).

102) Rae, S.C., and Burnett, K., Phys. Rev. A, **44**, 3835 (1991).

103) Reiss, H. R., J. Opt. Soc. Am. B, **4**, 726 (1987).

104) Rozmus, W., and Tikhonchuk, V.T., Phys. Rev. A, **42**, 7401 (1990).

105) Rulliere, C., Femtosecond laser pulses: principles and experiments, Springer, New York, 2004.

106) Sahyun, M. R. V., Hill, S. E., Serpone, N., Danesh, R., Sharma, D. K., J. Appl. Phys., **79**, 8030 (1996).

107) Said, A. A., Wamsley, C., Hagan, D. J., Van Stryland, E. W., Reinhardt, B. A., Roderer, P., Dillard, A. G., Chem. Phys. Lett., **228**, 646 (1994).

108) Salin, F., Squier, J., and Piche, M., Opt. Lett., 16, 1674 (1991).

109) Sandhu, A. S., and Kumar, G. R., Sengupta, S., Das, A. and Kaw, P.K., Phys. Rev. Lett., **95**, 025005 (2005).

110) Scalora, M., Dowling, J. P., Bowden, C. M., and Bloemer, M. J., J.Appl.Phys. **76**, 2023 (1994).

111) Scalora, M., Dowling, J. P., Bowden, C. M., and Bloemer, M. J., Phys.Rev.Lett. **73**, 1368 (1994).

112) Schoenlein, R. W., Lin, W. Z., Fujimoto, J. G., Eesley, G. L., Phys. Rev. Lett., **58**, 1680 (1987).

113) Siders, C. W., LeBlanc, S. P., Fisher, D., Tajima, T., Downer, M. C., Babine, A., Stephanov, A., Sergeev, A., Phys. Rev. Lett., **76**, 3570 (1996).

114) Seidemann, T., M. Yu. Ivanov, and P. B. Corkum, Phys. Rev. Lett., **75**, 2819 (1995).

115) Shakeshaft, R., J. Opt. Soc. Am. B, **4**, 705 (1987).

116) Shank, C. V., and Ippen, E. P., Appl. Phys. Lett., **24**, 373 (1974).

117) Sheik-Bahae, M., Said, A. A., Wei, T. M., Hagan, D. J., Van Stryland, E. W., IEEE J. Quantum Electron., **26**, 760 (1990).

118) Shen, Y. R., The principles of nonlinear optics, John Wiley & Sons, New York, 1984.

119) Siegman, A. E., Lasers, Oxford University Press, Oxford, 1986.

120) Smith, B. A., Zhang, J. Z., Giebel, U., Schmid, G., Chem. Phys. Lett., 270, 139 (1997).

121) Spence, D.E., Kean, P.N., Sibbett, W., Opt. Lett., **16**, 42 (1991).

122) Steinmeyer, G., Sutter, D. H., Gallmann, L., Matuschek, N., Keller, U., Science, **286**, 1507 (1999).

123) Strickland, D., and Mourou, G., Opt. Commun., **56**, 219 (1985).

124) Stuart, B. C., Feit, M. D., Herman, S., Rubenchik, A. M., Shore, B. W., and Perry, M. D., Phys. Rev. B, **53**, 1749 (1996).

125) Sun, Y. P., Riggs, J. E., Rollins, H. W., Guduru, R., J. Phys. Chem. B, 103, 77 (1999).

126) Sutherland, R. L., Handbook of Nonlinear Optics, Marcel Dekker, NY, 1996.

127) Sutter, D. H., Steinmeyer, G., Gallmann, L., Matuschek, N., Morier-Genoud, F., and Keller, U., Scheuer, V., Angelow, G., and Tschudi, T., Opt. Lett., **24**, 631 (1999).

128) Symes, D. R., Comley, A. J., and Smith, R. A., Phys. Rev. Lett., **93**, 145004 (2004).

129) Tajima, T., and Dawson, J. M., Phys. Rev. Lett., **43**, 267 (1979).

130) Tom, R. T., Nair, A. S., Singh, N., Aslam, M., Nagendra, C. L., Philip, R., Vijayamohanan, K., Pradeep, T., Langmuir, **19**, 3439 (2003).

131) Trevino-Palacios, C.G., Stegeman, G.I., and Baldi, P., Opt.Lett. **21**, 1442 (1996).

132) Tudoran, C. S., Assion, A., Wollenhaupt, M., Winter, M., and Baumert, T., Appl. Phys. Lett., **88**, 261109 (2006).

133) Tutt, L. W., and Boggess, T. F., Prog. Quantum Electron., 17, 299 (1993).

134) Umstadter, D., Kim, J. K., and Dodd, E., Phys. Rev. Lett., **76**, 2073 (1996).

135) Ung, T., Liz-Marzan, L. M., Mulvaney, P., J. Phys. Chem. B, 103, 6770 (1999).

136) Valdmanis, J. A., and Fork, R. L., IEEE J. Quantum Electron., **22**, 112 (1986).

137) Vogel, A., Nahen, K., Theisen, D., and Noack, J., IEEE J. Selected topics in Quant. Electron. **2**, 847(1996).

138) Weingartshofer, A., Holmes, J.K., Caudle, G., Clarke, E.M., and Kruger, H., Phys. Rev. Lett., **39**, 269 (1977).

139) Williams, F., Varma, S. P., and Hillenius, S., J. Chem. Phys. **64**, 1549(1976).

140) Wood, W. M., Focht, G., and Downer, M. C., Opt. Lett., 13, 984 (1988).

141) Wood, W. M., Siders, C. W., and Downer, M. C., Phys. Rev. Lett., **67**, 3523 (1991).

142) Xu, L., Spielmann, C., and Krausz, F., Szipocs, R., Opt. Lett., **21**, 1259 (1996).

143) Yablonovitch, E., Phys. Rev. Lett., **60**, 795(1988).

144) Yariv, A., J. Appl. Phys., **36**, 388 (1965).

145) Yariv, A., Quantum Electronics, John Wiley & Sons, New York, 1985.

146) Zhou, H., Zhou, K. F., Hu, W., Guo, Qi, Lan, S., Lin, X. S., Gopal, A. V., J. Appl. Phys., **99**, 123111 (2006).

147) Zhong, C. J., and Maye, M. M., Adv. Mater., **13**, 1507 (2001).

148) Zhou, J.P., Taft, G., Huang, C.P., Murnane, M. M., and Kapteyn, H.C., Christov, I.P., Opt. Lett., **19**, 1149 (1994).

149) Zhu, S., and Shen, W., J. Opt. Soc. Am. B, **4**, 739 (1987).

Appendix - I

Rate Equation Analysis

This is the programme written for evaluating the rate equations (2.17 to 2.21) given in chapter two.

```
//*****************************************************************
// program for  rate equation analysis  in a four level system assuming two photon
//absorption followed by excited state absorption.
//*****************************************************************

#include<cstdlib>
# include<iostream>
# include<cmath>
using namespace std;

void rungku(double&, double&, double&, double&, double&, double[][1], float);
double deriv(int, float, double[][1], double[][1]);
int main()
{
float fwhm, peak,lamda, cuvthk,Lin_T;
float beamwt, multi, zmove, area, x2x, x3x, incr, tslc, beeta,hp,c_vacuum;
int no_points,piece,p;
double x1x,sigma_2pa,sigma_esa,sigma_single,tau2,tau3,tau4,refind,oldgndpop;

//*****************************************************************
//reading the various parameters. The units of parameters are to be changed to
//make the calculation easy. length basic unit : micrometers, time basic unit:
//nanosecond, energy basic unit : microjoules
//*****************************************************************

no_points=85;          //no. of rows in the corresponding origin file
beamwt=17.0;           //beamwaist radius in micrometers
fwhm=7.0;              //FWHM of the pulse in nanoseconds
oldgndpop=1.452e4;     //groundstate population per cubic micron
tau2=100.0e-3;         //lifetime of level 2 in nanoseconds
tau3=1.4e-3;           //lifetime of level 3 in nanoseconds
tau4=0.6e-3;           //lifetime of level 4 in nanoseconds
sigma_esa=9.0e-8;      //ESA cross section (level 2 to level3) as micron^2
beeta=10.0e-2;         //2PA coefficient(micrometers/microjoules/nano seconds)
cuvthk=1e3;            //cuvette thickness in micrometers
lamda=532e-3;          //wavelength in micrometers
refind=1.2;            //refractive index of the solution
```

```
hp=6.626e-19;          //plank's constant in microJoules* nanoseconds
c_vacuum=3e5;          //velocity of light in vacuum in micrometers/nanoseconds
Lin_T=1;               //linear transmittance
p=8;                   //no of cuvette slices needed
tslc=((cuvthk*refind)/c_vacuum)/p;
piece=p;               //cuvette slices


//*****************************************************************
//reading the energy reaching the cuvette at each z position from the input file,
//where it is stored from the experimental origin file
//*****************************************************************

float enerpp[no_points], exp_nor_trans[no_points],exp_trans[no_points],
exp_nor_z[no_points];
int j1=0, zn;

for(int w=0; w<no_points; w++)
{
cin>>enerpp[w]>>exp_nor_trans[w]>>exp_nor_z[w];
j1=j1++;
exp_trans[w]=Lin_T*exp_nor_trans[w];
}

zn=j1;  //total number of points in the experimental points

//*****************************************************************
//calculation of 2PA cross section from Beeta & linear abs. cross section from
//linear transmission
//*****************************************************************

sigma_2pa=hp*c_vacuum*beeta/(lamda*oldgndpop);        //unit in
                                                      //micron^4*nanosecon
                                                      ds
sigma_single=log((1.0/Lin_T))/(oldgndpop*cuvthk);     //unit is micron^2

//*****************************************************************

int xy;
double outpeak[zn],outenerden[zn],
noutenerden[zn],outenergy[zn],nor_trans[zn],out_trans[zn];
float inpeak[zn], inenerden[zn],area_1[zn];
double cuvette[4][piece];

for (int p=0; p<zn; p++)
{
zmove=exp_nor_z[p];
```

```
x1x=1.0+(((zmove*lamda)/(3.14*beamwt*beamwt))*((zmove*lamda)/(3.14*bea
mwt*beamwt)));
multi=beamwt*sqrt(x1x);      //beam radius at different z positions
area=3.14*multi*multi/2.0;   //area of the gaussian beam at each z position
x2x=enerpp[p]/area;          //here the energy per pulse is taken as the
                             //experimental value of energy at the cuvette so that
                             //the pulse to pulse energy variation can be taken
                             //into account
area_1[p]=area;
x3x=x2x/fwhm;
inenerden[p]=x2x;            //input energy density at each z position
inpeak[p]=x3x;               //input peak intensity at each z position
}

double a1, b1, c1, d1,e1,e;
float nue;
int ntslice, argue;
nue=c_vacuum/lamda;

//*****************************************************************
//evaluation of the coefficients of the rate equation
//*****************************************************************

a1=sigma_2pa/(2.0*hp*hp*nue*nue);
b1=1/tau2;
c1=sigma_esa/(hp*nue);
d1=1/tau3;
e1=1/tau4;
e=hp*nue;

//*****************************************************************
// The array nonvbl stores the constants that are needed in the evaluation of the
//derivatives
//*****************************************************************
double nonvbl[9][1];
nonvbl[0][0]=a1;
nonvbl[1][0]=b1;
nonvbl[2][0]=c1;
nonvbl[3][0]=d1;
nonvbl[4][0]=e1;
nonvbl[5][0]=refind;
nonvbl[6][0]=sigma_2pa;
nonvbl[7][0]=sigma_esa;
nonvbl[8][0]=e;

//*****************************************************************
//checking the time slice length & calculating no. of slices
```

```
//*****************************************************************
float mu;
mu=(20.0/(2*tslc));
ntslice=int(2*mu);
argue=ntslice+1;
double intens[argue];          //this array keeps the intensity slices of each pulse
                               //that is calculated by using the gaussian expression
float t,t1, x, time[argue];
float calcu;
int j,k1;
j=int((argue/2.0)+0.5);

double outint[argue];          //this array keeps the output intensity of each
temporal
                               //slice of the pulse corresponding to the slice of the
                               //array intes[argue]
double n1, n2,n3,n4;
double new1, check, test=0.0;

if (tslc<=tau3)
{
for (int i=0; i<zn; i++)
{
peak=inpeak[i];          //assigning the peak experimental intensity at each z
position

//*****************************************************************
//calculating and storing the input intensity (getting the gaussian distribution of the
//temporal intesity of individual pulse)
//*****************************************************************

t=0.0, t1=0.0;

for (int k=(j-1); k<argue; k++)
{
x=(-1)*2*t*t/(fwhm*fwhm);
calcu=peak*exp(x);
intens[k]=calcu;
time[k]=t;
t=t+tslc;
}
for (int k=0; k<(j-1); k++)
{
intens[k]=intens[ntslice-k];
t1=t1-tslc;
k1=j-1-k;
time[k1]=t1;
```

```
}

//*****************************************************************
//calculating and storing the output intensity
//*****************************************************************
// for a four level system there are four coupled diff. equ. to be solved
//*****************************************************************

n1=oldgndpop;
n2=0.0;
n3=0.0;
n4=0.0;

for(int l=0; l<piece; l++)      //here the cuvette is getting sliced and each of the
                                //slice is filled with the different levels of population
{
cuvette[0][l]=n1;
cuvette[1][l]=n2;
cuvette[2][l]=n3;
cuvette[3][l]=n4;
}
check=0.0;              //the variable in which the peak output intensity is kept for a
                        //given pulse this is equivalent to the variable 'peak' for
                        //input intensity

for (int s=0; s<argue; s++)
{
new1=intens[s];                 //intensity of each of the time slice of the single
                                //gaussian pulse at each of the z position

for (int m=0; m<piece; m++)  //the logic of this m loop is that each of the intensity
                              //slice passes through each cuvette slice and getting
                             //modified from each. After the passing of a slice
                             //fully through the cuvette pieces the population in
                             //each of them will be modified. Then that intensity
                             //is kept in the outint array. Then the s loop takes the
                             //second intensity slice and passes it through the full
                             //cuvette slices.
{
rungku(cuvette[0][m],cuvette[1][m],cuvette[2][m],cuvette[3][m],new1,nonvbl,tslc
);

//this step means functioning of the mechanism in an actual system each of the
//small temporal slice passes through the whole cuvette slices and affects those
//populations. The next slice sees this population in the respective cuvette slices.
//The intensities then get affected by the populations. After the passage of a full
```

```
//pulse the populations get refreshed to the initial values and the cycle is repeated
//for the new pulse with a different  peak intensity. i.e. at a different z position.

if (cuvette[0][m]<test)
{
cout<<"n1 is becoming negative, change the input parameters,
especially,tau2,groundpop etc"<<endl;
exit(1);
}
else
{
if (cuvette[1][m]<test)
{
cout<<"n2 is becoming negative, change the input parameters,
especially,tau2,tau3,groundpop etc"<<endl;
exit(1);
}
else
{
if (cuvette[2][m]<test)
{
cout<<"n3 is becoming negative, change the input parameters, especially,
sigma_esa,tau3,tau4 etc"<<endl;
exit(1);
}
else
{
if(cuvette[3][m]<test)
{
cout<<"n4 is becoming negative, change the input parameters,
especially,sigma_esa,tau4 etc"<<endl;
exit(1);
}
else
{
if (new1<test)
{
cout<<"I is becoming negative, change the input parameters,
especially,sigma_esa,tau2,tau3,tau4,groundpop etc"<<endl;
exit(1);
}
else goto esc;
}
}
}
}
esc: continue;
```

```
}

outint[s]=new1;                 //output intensity after all the rate equation process
                                //corresponding to a single slice of a single pulse

{
check=outint[s];                //finds out the peak intensity of the output pulse
                                //corresponding to each pulse. The final value of the
                                //variable check will be the essential out put of the
                                //whole rate equation mechanism corresponding to a
                                //single pulse. After this the solution is theoretically
                                //brought back to the initial populations to be
                                //repeated for another pulse
}
}

outpeak[i]=check;
noutenerden[i]=check*fwhm;
outenergy[i]=noutenerden[i]*area_1[i];
        }                       //this i loop stands for one z position. After one
                                //execution the entire thing repeats for the next z
                                //position.

double check_1=0.0;
for(int p=0; p<zn; p++)
{
if(outenergy[p]>check_1)
{
check_1=outenergy[p];
}
}

for(int i=0; i<zn; i++)
{
nor_trans[i]=outenergy[i]/check_1;  //This is calculated by taking the assumption
                                    //that nor_trans = the output energy/max.
output
                                    //energy
out_trans[i]=outpeak[i]/inpeak[i];  //This is done by taking transmittance
                                    //(theoretical) =output peak intensity/input
                                    //peak intensity at each of the z position

cout<<inpeak[i]<<"\t"<<outpeak[i]<<"\t"<<inenerden[i]<<"\t"<<exp_nor_trans[i]
<<"\t"<<nor_trans[i]<<"\t"<<exp_trans[i]<<"\t"<<out_trans[i]<<"\t"<<endl;

}
cout<<"no. of rows of origin file"<<"\t"<<no_points<<endl;
```

```
cout<<"beamwaist in micrometers"<<"\t"<<beamwt<<endl;
cout<<"FWHM  in nanoseconds"<<"\t"<<fwhm<<endl;
cout<<"N1 as per micron^3"<<"\t"<<oldgndpop<<endl;
cout<<"tau2- level 2 to the level1 in nanoseconds"<<"\t"<<tau2<<endl;
cout<<"tau3- level 3 to the level2 in nanoseconds"<<"\t"<<tau3<<endl;
cout<<"tau4- level 4 to the level3 in nanoseconds"<<"\t"<<tau4<<endl;
cout<<"excited state abs. cross section  as micron^2"<<"\t"<<sigma_esa<<endl;
cout<<"2PA
coefficient(micrometers/microjoules/nanoseconds)"<<"\t"<<beeta<<endl;
cout<<"2PA abs. cross section in micron^4nanoseconds\t"<<sigma_2pa<<endl;
cout<<"linear abs. cross section  as micron^2"<<"\t"<<sigma_single<<endl;
cout<<"cuvette thickness in micrometers"<<"\t"<<cuvthk<<endl;
cout<<"wavelength in micrometers"<<"\t"<<lamda<<endl;
cout<<"refractive index of the solution"<<"\t"<<refind<<endl;
cout<<"timeslice in nanoseconds"<<"\t"<<tslc<<endl;
cout<<"Linear transmittance of th sample"<<"\t"<<Lin_T<<endl;
//} //if loops ends
else
cout<<"time slice greater than relaxation times!define tslc to a lower
value"<<endl;
return 0;
}
void rungku(double& y1, double& y2, double& y3,double& y4, double& x,
double m1[][1], float tslc)
{
double res[5][1], res1[5][1], res2[5][1], res3[5][1], resul[5][5];
float t1=0.0;
res[0][0]=y1;  //the array res is having the pupulation of the four levels
               //and the intensity of each time slice of each pulse as
               //the elements(intial values)
res[1][0]=y2;  //N2(initial)
res[2][0]=y3;  //N3(initial)
res[3][0]=y4;  //N4(initial)
res[4][0]=x;   //intensity at the cuvette of each time slice of a given pulse
               //res[][] is yn

for (int j=0; j<5; j++)
{
resul[j][0]=tslc*deriv(j,t1,res,m1);    //mainly the population of each cuvette
                                        //slice and the nonvariables are passed
                                        //to the function deriv
                                        //k1,l1,m1,s1&o1
                                        //for j=0, deriv : f()
                                        //for j=1, deriv : g()
                                        //for j=2, deriv : p()
                                        //for j=3, deriv : q()
                                        //for j=4, deriv : r()
```

```
}
t1=t1+tslc/2.0;
for(int j=0; j<5; j++)
{
res1[j][0]=res[j][0]+(resul[j][0]/2.0); //n1+k1/2,n2+l1/2,n3+m1/2,n4+s1/2,I+o1/2
}
for(int j=0; j<5; j++)
{
resul[j][1]=tslc*deriv(j,t1,res1,m1);   //k2,l2,m2,s2&o2
}
for(int j=0; j<5; j++)
{
res2[j][0]=res[j][0]+(resul[j][1]/2.0); //n1+k2/2,n2+l2/2,n3+m2/2,n4+s2/2,I+o2/2

}
for(int j=0; j<5; j++)
{
resul[j][2]=tslc*deriv(j,t1,res2,m1);   //k3,l3,m3,s3,o3
}
t1=t1+tslc/2.0;
for(int j=0; j<5; j++)
{
 res3[j][0]=res[j][0]+resul[j][2];        //n1+k3,n2+l3,n3+m3,n4+s4,I+o3
}
for(int j=0; j<5; j++)
{
 resul[j][3]=tslc*deriv(j,t1,res3,m1);  //k4,l4,m4,s4,o4
}
for(int j=0; j<5; j++)
{
 resul[j][4]=res[j][0]+((resul[j][0]+2*(resul[j][1]+resul[j][2])+resul[j][3])/6.0);

                                //this array stores the final values of the populations
}

//*****************************************************************
y1=resul[0][4];          //N1
y2=resul[1][4];          //N2
y3=resul[2][4];          //N3
y4=resul[3][4];          //N4
x=resul[4][4];           //solved intensity

}//At the end of the rengku function running for once, the population of each
//cuvette slice changes and the fuction returns the changed intensity if the slice
//calculted from the changed populations.

//*****************************************************************
```

```
//function to evaluate the derivative
//*************************************************************

double deriv(int k, float t1, double p1[][1], double p2[][1])
                    //for a given input intensity slice this function just evaluates the
                    //different fuctions and returns that value to the rengku function.
{
double r, rx, ry, rz,rt, rw;

switch (k*10)
{
case 0:
rx =-p2[0][0]*(p1[0][0]-p1[2][0])*p1[4][0]*p1[4][0]+p2[1][0]*p1[1][0];   //f()
r=rx;
break;
//
case 10:
ry=-p2[2][0]*(p1[1][0]-p1[3][0])*p1[4][0]-
p2[1][0]*p1[1][0]+p2[3][0]*p1[2][0]+p2[4][0]*p1[3][0];                   //g()
r=ry;
break;
//
case 20:
rz=p2[0][0]*(p1[0][0]-p1[2][0])*p1[4][0]*p1[4][0]-p2[3][0]*p1[2][0];     //p()
r=rz;
break;
//
case 30:
rt=p2[2][0]*(p1[1][0]-p1[3][0])*p1[4][0]-p2[4][0]*p1[3][0];              //r()
r=rt;
break;
//
case 40:
rw=-(3e5/p2[5][0])*(((p2[6][0]*(p1[0][0]-
p1[2][0])*p1[4][0]*p1[4][0])/p2[8][0])+p2[7][0]*(p1[1][0]-
p1[3][0])*p1[4][0]);//q()
r=rw;
break;
}
return r;
}
```

Appendix - II

Light Propagation through Nonlinear Media Arranged in Tandem

(a) Matlab programme for the forward biased condition (Saturable absorber followed by reverse saturable absorber) as given in chapter three.

```
%case 1: SA followed by RSA
%non_linear_sample_SA_RSA_P.m

function non_linear_sample_SA_RSA_P

% evaluation of transmission in materials with linear saturable absorption and
%two photon absorption samples put in tandem

a=load('input.txt');
energy=a(:,1);
expt_nor_trans=a(:,2);
z_position=a(:,3);

[m,n]=size(a);

%input variabes
global T_SA T_RSA L_SA L_RSA beeta Isat
omega0=50e-6;       % beam waste radious in meters
lamda=532e-9;       % excitation wavelength in meters
tau=7-9;            %  input laser pulse width
tslc=7e-10;         % decides the total number of temporal slices of each of the
                    %input pulse till the fwhm(pulse width)
L_SA=1e-3;          %length of the sample through which the pulse is passing
                    %(Saturable Absorber)
L_RSA=1e-3;         %length of the sample through whcih the pulse is passing
                    %(Reverse Saturable Absorber)

T_SA=0.1;%          % Linear transmission measured before the lens (Saturable
Absorber)
T_RSA=0.1;          % Linear transmission measured before the lens (Saturable
                    %Absorber)
Lin_T=T_SA*T_RSA;
No=100;             % number of steps needed in the runge-Kutta evluatio of
                    %the propagation through the sample of length L (total
                    %length/No=stepsize for the Runge-Kutta)
```

```
beeta=5.0e-11;          % 2PA absorption coefficient in m/W
Isat=15.0e12;           % saturation intensity in W/m2
h1=L_SA/No;             %step size in Runge-Kutta (SA material)
h2=L_RSA/No;            %step size in Runge-Kutta (RSA material)
mu=tau/tslc;
j=mu/2;                 %works for total even number of time slices
                        %calculates the peak intensity at each z position
for i=1:m
omega(i)=omega0*sqrt((1+((lamda*z_position(i)*1e-
6)/(pi*omega0*omega0))^2));
gauss=4*(sqrt((log(2)/pi)));
Ipeak(i)=(gauss*energy(i)*1e-6)/(pi*omega(i)*omega(i)*tau);
                        %for a gaussian beam

 peak=Ipeak(i);
 t=0.0;
 outfluence_1=0.0;
 influence=0.0;

  for k=j+1
  while k<=(mu+1),
        x=(-1)*2*t*t/(tau*tau);
        calcu=peak*exp(x);
  intens(k)=calcu;
  t=t+tslc;
  k=k+1;
        end
        end

        for k=1
    while k<=j,
      intens(k)=intens(mu+2-k);
  k=k+1;
        end
end

%case 1: SA followed by RSA

 for k=1:(mu+1)
     pass=intens(k);
     x=0;
  for l=1:No
  k1=h1*rk4(x,pass);
  k2=h1*rk4(x+h1/2,pass+k1/2);
  k3=h1*rk4(x+h1/2,pass+k2/2);
  k4=h1*rk4(x+h1,pass+k3);
  pass=pass+(1/6)*(k1+2*k2+2*k3+k4);
```

```
  x=x+h1;
        end
  outintens(k)=pass;
end

for k=1:(mu+1)
     pass_1=outintens(k);
     x=0;
  for l=1:No
  k1=h2*rk4_1(x,pass_1);
  k2=h2*rk4_1(x+h2/2,pass_1+k1/2);
  k3=h2*rk4_1(x+h2/2,pass_1+k2/2);
  k4=h2*rk4_1(x+h2,pass_1+k3);
  pass_1=pass_1+(1/6)*(k1+2*k2+2*k3+k4);
  x=x+h2;
        end
  outintens_1(k)=pass_1;
end


%integrating the output and input intensities using trapezoidal rule

for o=1
  while o<=mu,
    outfluence_1=outfluence_1+tslc*((outintens_1(o)+outintens_1(o+1))/2);
    influence=influence+tslc*((intens(o)+intens(o+1))/2);              %J/m^2
  o=o+1;
end
end

%Assigning the X and Y values to plot

  X(i)=z_position(i);
  influe(i)=influence;
  outflue_1(i)=outfluence_1;
  Trans(i)=outflue_1(i)/influe(i);
  Y(i)=Trans(i)/Lin_T;
end

X1=X';
Y1=Y';
plot(X,Y)

fid1=fopen('fluenceout.dat','w');
for p=1:m
  fprintf(fid1,'%9.4f\t%9.4f\t%9.4f\t%9.4e\n',X(p),a(p,2),Y(p),Trans(p));
end
```

```
  fprintf(fid1,'wavelength=%9.4f nm\n',lamda*1e9);
  fprintf(fid1,'pulse width=%9.4f fs\n',tau*1e15);
  fprintf(fid1,'omega zero=%9.4f microns\n',omega0*1e6);
  fprintf(fid1,'linear transmission=%9.4f\n',T);
  fprintf(fid1,'sample length=%9.4f microns\n',L*1e6);
  fprintf(fid1,'beeta=%9.4e x 1e-12 m/W\n',beeta*1e12);
  fprintf(fid1,'Isat=%9.4f x 1e15 W/m^2\n',Isat*1e-15);
fclose(fid1);


function result=rk4(x1,y1)
global T_SA L_SA  Isat
alpha0SA=(log((1/T_SA)))/L_SA;
result=-((alpha0SA/(1+(y1/Isat))))*y1;

function result1=rk4_1(x2,y2)
global beeta T_RSA L_RSA
alpha0RSA=(log((1/T_RSA)))/L_RSA;
result1=-alpha0RSA*y2-beeta*y2*y2;
```

(b) Matlab programme for the reverse biased condition (Reverse saturable absorber followed by saturable absorber) as given in chapter three.

```
%case 2: RSA followed by SA
%non_linear_sample_RSA_SA_B.m

function non_linear_sample_RSA_SA_B

a=load('input.txt');
energy=a(:,1);
expt_nor_trans=a(:,2);
z_position=a(:,3);

[m,n]=size(a);

%input variabes
global T_SA T_RSA L_SA L_RSA beeta Isat
omega0=50e-6;          % beam waste radious in meters
lamda=532e-9;          % excitation wavelength in meters
tau=7e-9;              %  input laser pulse width
tslc=7e-10;            % decides the total number of temporal slices of each of
                       %the input pulse till the fwhm(pulse width)
```

```
L_SA=1e-3;          %length of the sample through whcih the pulse is passing
                    %(Saturable Absorber)
L_RSA=1e-3;         %length of the sample through whcih the pulse is passing
                    %(Reverse Saturable Absorber)
T_SA=0.1            % Linear transmission measured before the lens (Saturable
                    %Absorber)
T_RSA=0.1;          % Linear transmission measured before the lens ( Reverse
                    %Saturable Absorber)
Lin_T=T_SA*T_RSA;
No=100;             % number of steps needed in the runge-Kutta evluatio of
                    %the propagation through the sample of length L (total
                    %length/No= stepsize for the Runge-Kutta)
beeta=5.0e-11;      % 2PA absorption coefficient in m/W
Isat=15e12;         % saturation intensity in W/m2
h1=L_RSA/No;        %step size in Runge-Kutta (for RSA, first, material)
h2=L_SA/No;         %step size in Runge-Kutta (for SA, second, material)
mu=tau/tslc;
j=mu/2;             %works for total even number of time slices

%calculates the peak intensity at each z position
for i=1:m
omega(i)=omega0*sqrt((1+((lamda*z_position(i)*1e-
6)/(pi*omega0*omega0))^2));
gauss=4*(sqrt((log(2)/pi)));
Ipeak(i)=(gauss*energy(i)*1e-6)/(pi*omega(i)*omega(i)*tau);%for a gaussian
beam

peak=Ipeak(i);
t=0.0;
outfluence_1=0.0;
influence=0.0;

  for k=j+1
  while k<=(mu+1),
        x=(-1)*2*t*t/(tau*tau);
        calcu=peak*exp(x);
  intens(k)=calcu;
  t=t+tslc;
  k=k+1;
        end
        end

        for k=1
    while k<=j,
      intens(k)=intens(mu+2-k);
  k=k+1;
        end
```

```
end

%case 2: RSA followed by SA

  for k=1:(mu+1)
      pass=intens(k);
      x=0;
   for l=1:No
   k1=h1*rk4(x,pass);
   k2=h1*rk4(x+h1/2,pass+k1/2);
   k3=h1*rk4(x+h1/2,pass+k2/2);
   k4=h1*rk4(x+h1,pass+k3);
   pass=pass+(1/6)*(k1+2*k2+2*k3+k4);
   x=x+h1;
          end
   outintens(k)=pass;
end

for k=1:(mu+1)
      pass_1=outintens(k);
      x=0;
   for l=1:No
   k1=h2*rk4_1(x,pass_1);
   k2=h2*rk4_1(x+h2/2,pass_1+k1/2);
   k3=h2*rk4_1(x+h2/2,pass_1+k2/2);
   k4=h2*rk4_1(x+h2,pass_1+k3);
   pass_1=pass_1+(1/6)*(k1+2*k2+2*k3+k4);
   x=x+h2;
          end
   outintens_1(k)=pass_1;
end


%integrating the output and input intensities using trapezoidal rule

for o=1
   while o<=mu,
     outfluence_1=outfluence_1+tslc*((outintens_1(o)+outintens_1(o+1))/2);
     influence=influence+tslc*((intens(o)+intens(o+1))/2);%J/m^2
   o=o+1;
end
end

%Assigning the X and Y values to plot

   X(i)=z_position(i);
   influe(i)=influence;
```

```
   outflue_1(i)=outfluence_1;
   Trans(i)=outflue_1(i)/influe(i);
   Y(i)=Trans(i)/Lin_T;
 end

X1=X';
Y1=Y';
plot(X,Y)

fid1=fopen('fluenceout.dat','w');
for p=1:m
   fprintf(fid1,'%9.4f\t%9.4f\t%9.4f\t%9.4e\n',X(p),a(p,2),Y(p),Trans(p));
end
   fprintf(fid1,'wavelength=%9.4f nm\n',lamda*1e9);
   fprintf(fid1,'pulse width=%9.4f fs\n',tau*1e15);
   fprintf(fid1,'omega zero=%9.4f microns\n',omega0*1e6);
   fprintf(fid1,'linear transmission=%9.4f\n',T);
   fprintf(fid1,'sample length=%9.4f microns\n',L*1e6);
   fprintf(fid1,'beeta=%9.4e x 1e-12 m/W\n',beeta*1e12);
   fprintf(fid1,'Isat=%9.4f x 1e15 W/m^2\n',Isat*1e-15);
fclose(fid1);


function result=rk4(x2,y2)
global beeta T_RSA L_RSA
alpha0RSA=(log((1/T_RSA)))/L_RSA;
result=-alpha0RSA*y2-beeta*y2*y2;

function result1=rk4_1(x1,y1)
global T_SA L_SA  Isat
alpha0SA=(log((1/T_SA)))/L_SA;
result1=-((alpha0SA/(1+(y1/Isat))))*y1;
```
